Worcester Polytechnic Institute
Digital WPI

Major Qualifying Projects (All Years)

Major Qualifying Projects

April 2009

Thin-Film Ferrofluidics

Dante Amoroso
Worcester Polytechnic Institute

Nicholas Bradley LeCompte
Worcester Polytechnic Institute

Follow this and additional works at: https://digitalcommons.wpi.edu/mqp-all

Thin-film Ferrofluidics

Dante Amoroso and Nicholas LeCompte

April 29, 2009

Contents

Acknowledgments

We would like to thank our advisors, Professors Iannacchione and Vernescu, for their guidance and support in this project. We would also like thank Professors Luo and Weekes and Gerardo Hernández for teaching us mathematical fluid mechanics in D Term 2008.

Dante thanks Professor Jacques Amar at the University of Toledo for teaching him techniques in computational physics. He would especially like to thank his fiancée Tanya Kiacolai for (inexplicably) putting up with him.

Nick thanks Professor Daniel Lathrop at the University of Maryland for introducing him to problems in Laplacian growth and Hele-Shaw flow.

Abstract

Ferrofluids are novel materials made up of nanoscale ferromagnetic particles (usually simply iron) suspended in an organic solvent (usually an ordinary oil). The resulting material remains a liquid but becomes susceptible to magnetic forces as well. This leads to a system which obeys both the laws of fluid dynamics simultaneously to those of magnetism which in turn causes some very strange and unique behaviors on the part of the fluid. In particular, experiments on ferrofluids in thin films have resulted in a wide array of exciting and mysterious morphologies.

We present several examples of interesting phenomena seen only in ferrofluidics, and then proceed to specialize to one experimental set-up for the purposes of modeling. We consider first the case of ferrofluid in a Hele-Shaw cell two panes of glass a short distance apart wherein the ferrofluid is deposited before application of magnetic field. This leads to an essentially two dimensional case to which we apply a constant magnetic field perpendicular to the plane of the cell, and then a spatially uniform magnetic field transverse to the cell, the direction of which rotates continuously in time. A number of experimental groups have studied this configuration, and we seek to develop a theoretical framework which reproduces observed evolution of the system.

The Navier-Stokes equations for ferrofluids are then developed. The basic steps are similar to the traditional Navier-Stokes equations, but now feature the addition of various electromagnetic terms. The resulting system has significantly more unknowns than equations, but is almost fully specified by the removal of electric terms and the specialization to two dimensions, both of which are justified by our specific case. Using this equation, we derive a model similar to Darcy's law and formulate the necessary boundary conditions.

The major problem then becomes two-fold. We first decouple the equation governing the magnetization internal to the fluid, and develop two models for its behavior. Numerical solutions are obtained for both cases and discussed and compared. The second part of the problem is the use of a vortex sheet method to develop a governing equation for the curvature along the boundary of the fluid. By taking a limiting no-slip case, an equation involving no unknowns is obtained.

Finally, we consider a moving boundary value problem governing the pressure. By incompressibility, the pressure obeys a Laplace equation, but the movement of the ferrofluid implies that our domain is not constant, which significantly complicates the problem. We formulate the problem so that classical solutions are given as a pair; the pressure which satisfies the partial differential equation, and a diffeomorphism of the boundary which describes how the fluid itself moves. These two functions are coupled by a boundary condition which specifies that the gradient of the pressure is related to the velocity of the moving boundary. We discuss the problem of existence of classical solutions to this moving boundary value problem, and show that classical solutions are volume-preserving.

Chapter 1

Introduction

Ferrofluids are liquids with nanoscale ferromagnetic particles suspended within them. This configuration results in materials which obey both the laws of fluid mechanics, and those of magnetism[1]. A problem of considerable interest is thus how ferrofluids move while under the influence of a given magnetic field. This area of study is called ferrohydrodynamics.

We use the term *ferrofluidics* rather than *ferrohydrodynamics* in our report because we do not focus on general properties of the flow of ferrofluids. Rather, we are interested in creeping velocity behavior; flow at very low Reynolds number and in a quasi-static limit. In particular, the type of behavior we are interested in is rife with potential applications - the ability to precisely control small volumes of fluid is a long-term goal for the general study of *fluidics*, the science of controlling fluids precisely, with the motivating application of performing operations similar to that of electronic circuits. Here we list a few notable applications of ferrofluids [14]:

- Companies such as Ferrotec have been using ferrofluids to form a seal between rotating discs, particularly in hard drives. Magnets hold the fluid in place and reduce the viscosity, creating a low-friction, effective seal.

- Medical researchers are currently interested in applying ferrofluids to detect and remove tumors by carefully controlling a volume through the body.

- Ferrari has recently used magnetorheological fluid (similar to ferrofluid, but with coarser grains that result in a bulk-chain effect under application of a magnetic field)

---

[1]Specific details on the makeup of ferrofluids will be given in Section 2.2.

in the suspension of some of their cars. Other mechanical engineering groups are interested in the friction-reducing capability of ferrofluids under certain applied magnetic fields.

Furthermore, as the study of ferrofluids is only forty years old [23], we expect new and exciting applications to be developed within the next few decades.

Beyond this, the study of pattern formation in ferrofluids is of considerable physical interest. In two dimensions, which we focus on almost exclusively in this paper, a number of similarities to Hele-Shaw flow are seen[2], particularly the Saffman Taylor instability [25]. Figure 1.1 demonstrates some examples particularly nicely. Ferrofluids have a tendency to undergo viscous fingering [6][4] and form labyrinthine patterns [13]. A number of questions can be asked about the nature of the resulting patterns [9][12][17], but we will choose to focus instead on the dynamics actually causing the formation of these structures.

Figure 1.1: This figure, taken from http://www.eecs.mit.edu/grad/area4/subjects.html, demonstrates some major features seen in thin-film ferrofluids. The initial image shows a starting ferrofluid volume. After some magnetic fields are applied, fingering begins in the second image, eventually resulting in curled fingers in the third. The last two images show the result of a greater initial volume of ferrofluid, where the interior of the liquid assumes the morphology of multiple, disconnected droplets with a labyrinthine structure in between them.

We first spend a fair amount of time deriving the basic governing equations and explaining the fundamental physical issues at hand. While much of this is somewhat elementary, it is also a poorly-understood area of physics that demands careful exposition. In particular, anything below a thorough discussion of the physical principles could obscure the phenomena

---

[2]Again, more details follow in Section 2.6.

7

we attempt to describe. For example, many briefer surveys tacitly assume collinearity of the magnetization and applied magnetic fields, which eliminates some important characteristics of the motion. We've also found some disagreement as to the role that the kinematics of the suspended magnetic particles play in the dynamics of the bulk fluid, as well as inconsistencies between different authors both in notation and nomenclature. As a result, part of our initial aim is in establishing a clear physical grounding and fixing an internally consistent system of definitions and symbols. We also give a brief discussion on general principles of fluid mechanics and magnetization, primarily for the benefit of our intended audience; people who are familiar with vector analysis, classical mechanics and electrodynamics, and dynamical systems, but who may not be familiar with continuum mechanics and magnetism.

The next chapter is spent deriving and discussing our model. We extend a well-studied model known as Darcy's law, which specifies that a fluid in a thin film moves linearly with respect to the gradient of a (generalized) pressure. Our main result here is the addition of a torque term which cannot be expressed as the gradient of a scalar. After developing this model we take some time to decouple an evolution equation for the magnetization of the ferrofluid and study it both analytically and numerically following several models. From here we proceed to a vortex sheet formulation of the problem of the evolution of the curvature of the boundary of the domain of the ferrofluid in our model. By enforcing continuity of velocity across the boundary, we obtain a differential equation for the curvature. Lastly, we finish with an explicit moving boundary problem for the ferrofluid time development, and discuss its physical relevance.

Chapter 2

Basic Theory of Ferrofluidics

Most of sections 2.1-2.3 follow closely with the text by Rosensweig [22]. We present the material here in a summary form for readers unacquainted with the various basic concepts set forth, but who do not wish to read through the book themselves. In sections 2.4 and 2.5 we also present a number of results from Odenbach [14] in addition to more from Rosensweig, for the same reasons.

2.1   Principles of Magnetism

2.1.1   Magnetic Materials

There are several different types of behavior that magnetically interacting materials can present, and in order to discuss the nature of the magnetic interactions the particles in a ferrofluid experience, it will be useful to briefly summarize these types of behavior. The first three of these rely on an understanding of the configurations of magnetic moments of atoms in solids, and so we'll begin there.

All solid matter consists of atoms arranged in some sort of crystalline structure. Within a large amount of matter there may be multiple sets of crystals, where the regular pattern of one region of crystal is broken along a line and the pattern of the adjacent region begins. The sizes of these regions can vary greatly depending upon the type of material, and it is even possible for the entire piece of solid matter to consist of a single crystal.

Each of the atoms in these crystal structures has a magnetic moment associated with it,

and depending on the specific structure in the particular region of the crystal, a number of these magnetic moments may be aligned. The regions where all the magnetic moments of individual atoms are oriented in a given direction are called magnetic domains. Each region of crystal can have multiple domains inside it, and so a solid that is just a single crystal may still be comprised of multiple magnetic domains. These domains arise from the fact that alignment between close magnetic moments places a lot of energy into the magnetic field, but the thin regions separating different domains are also energetically unfavorable, so materials tend to assume an intermediate size for domains where all moments are aligned. It is worth noting, however, that it is possible to take a piece of material so small that all the atoms are part of the same domain.

Now that the concept of domains and magnetic moments has been introduced, the types of magnetic behavior exhibited by materials can be explained. The first of these is Ferromagnetism. In ferromagnetic materials it is energetically favorable for the atoms to have their magnetic moments aligned. This results in a material with a very large net magnetic moment in the favorable direction.

The opposite of ferromagnetic materials are anti-ferromagnetic materials, wherein a lack of net magnetic moment is most favorable. These materials are unaffected by magnetic fields. Similar to antiferromagnetism is ferrimagnetism. Ferrimagnetic materials exhibit magnetic moments which are unaligned, but the magnitudes of the moments are larger along certain preferred directions. These materials retain a net magnetic moment as a result, but typically to a lesser degree than ferromagnetic materials.

The last two types of interactions, paramagnetism and diamagnetism, do not arise from materials with domains built into their structure, but are instead dependent on external applied magnetic fields. In paramagnetic materials an applied field will cause the magnetic moments to align themselves with it, but without long-range ordering. This behavior is seen in a number of materials under all conditions, as well as in ferromagnets which have been heated to the point that they lose their natural internal alignment. Diamagnetism is essentially the opposite, wherein an applied magnetic field causes the moments to align opposite the field, again without long-range order.

In ferrofluids, single domain ferro- or ferrimagnetic particles are placed in a colloidal

10

suspension. These is no long-range ordering present in this arrangement. The result of this construction is that the material as a whole exhibits a type of paramagnetism termed superparamagnetism. The behavior is the same as that of paramagnetism except that larger magnetization results from the applied fields than is typical of these materials.

2.1.2 Laws Governing Magnetism

We begin our discussion of the nature of magnetic forces by defining various terms such as 'magnetic field', 'induction field', 'magnetization' etc. (some of which have already been used) formally.

Magnetic Field Although no isolated magnetic poles have been seen in nature, it is useful to build our discussion of magnetic forces using the concept of a magnetic pole. These poles come in two 'signs': north and south, and behave similar to electric charge in that like poles repel while unlike poles attract. The magnitude of the force between two poles of strength p and p' follows an inverse square relation resulting in the magnitude of the force being given by $pp'/4\pi\mu_0 r^2$, where r is the distance between the poles and μ_0 is the permeability of free space, having the value $\mu_0 = 4\pi \times 10^{-7}$.

If p' is of unit magnitude and north, the force it experiences is called the magnetic field, represented by $\mathbf{H}$. Note that as forces are vector quantities, so is the magnetic field. The direction of the magnetic field is thus along the vector from the position of p to p', picking up a negative sign if the p is south. We can thus write Eq. 2.1.1 to define magnetic fields, wherein we follow the usual convention $|\mathbf{r}| = r$ and $\hat{\mathbf{r}} = \mathbf{r}/r$.

$$\mathbf{H} = \frac{p\hat{\mathbf{r}}}{4\pi\mu_0 r^2} \tag{2.1.1}$$

Magnetization As noted in the previous section, many materials can exhibit an internal magnetic moment. We discuss this concept in terms of the quantity $\mathbf{M}$, the magnetization. For a pole of uniform strength p with a surface area a we define the intensity of the magnetization as $M = p/a\mu_0$ or $M = \rho_s/\mu_0$, where ρ_s is the surface density of magnetic poles.

Induction Field The induction field is a somewhat harder concept to build initially, so we shall approach it from the point of view of 'lines of induction'. In vacuum, we define the

induction field B to be $B = \mu_0 H$. Thus, the induction field surrounding a pole p has its magnitude given by $B = p/4\pi r^2$. If we imagine this induction field as lines radiating outward from the pole, unit intensity B is the case of one line of induction crossing one square meter of area oriented perpendicularly to the field lines. Each line of induction is the unit weber, represented by Wb, leading to the units of the induction field being Wb/m^2, also called tesla (T). Thus, a sphere surrounding our imaginary magnetic monopole p would be crossed by the number of lines $4\pi r^2 B$ which we note is also the magnitude of p. Thus the magnitude of a pole is representative of the number of lines of induction originating from it. This final point will allow us to bring B, H and M together to define the induction field when matter is involved.

We begin by considering the case of a ferromagnetic bar in a magnetic field $\mathbf{H}$ with the bar's own magnetization $\mathbf{M}$ (which has its direction given by the vector from the south pole to the north) oriented parallel to the magnetic field. If we remove a very thin cross-section from the center of the bar a pole will appear on either side of the resultant gap. Since every pole results in one induction line, symmetry dictates that $p/2a$ lines are caused by the north pole and $p/2a$ are caused by the south, where p is the strength of the original bar magnet and a is the area in the gap we've created. This gives a total $p/a = \rho_s = \mu_0 M$ induction lines produced by the bar magnet. The magnetic field across the entire gap produces another $\mu_0 H$ lines of induction, resulting in a total induction field given by $B = \mu_0 (M + H)$. Since this induction field remains the same if we close the gap again we conclude that the induction due to magnetization inside materials is oriented from south poles to north poles, while outside the bar magnet the induction field forms closed loops from the north pole to the south. We thus define the vector form of the induction field by Eq. 2.1.2.

$$\mathbf{B} = \mu_0 \left(\mathbf{H} + \mathbf{M} \right) \tag{2.1.2}$$

Magnetic Dipoles   As previously noted, lone magnetic poles are undiscovered in nature. Instead, all magnetic poles appear in pairs, called dipoles, of a north and a south pole of equal magnitude situated very close together. This concept is also true of matter exhibiting magnetization. In the case of a differential volume of this matter we can take $\mathbf{M}$ to be constant and find that the two ends of the volume have a surface pole density of $\pm\rho_s$, where positive represents north and negative represents south.

From here we will consider basic properties of magnetic dipoles. We call the vector

from the south poles to the north poles $\mathbf{d}$. This is then both a useful relation between the positions of the poles and a measure of the length of our differential volume. From here we are interested in the magnetic field produced by the dipole at a point far away from it. We consider the position relative to the dipole to be the position relative to the center of the dipole and call this $\mathbf{r}$. Thus the position relative to the negative pole is $\mathbf{r}_1 = \frac{1}{2}\mathbf{d} + \mathbf{r}$ while the position relative to the positive pole is $\mathbf{r}_2 = -\frac{1}{2}\mathbf{d} + \mathbf{r}$. Introducing a_d such that $V = a_d d$, implying that $a_d \rho_s$ is the magnitude of the poles, and applying the fact that $\hat{\mathbf{r}} = \mathbf{r}/r$ we substitute into Eq. 2.1.1 to get Eq. 2.1.3.

$$\mathbf{H(r)} = \frac{\rho_s a_d}{4\pi\mu_0} \left(-\frac{\mathbf{r}_1}{r_1^3} + \frac{\mathbf{r}_2}{r_2^3} \right) \tag{2.1.3}$$

If we call θ the angle between $\mathbf{d}$ and $\mathbf{r}$ and apply the condition that $d \ll r$ we can write

$$r_1 \approx r + \frac{d}{2}\cos\theta, \quad r_2 \approx r - \frac{d}{2}\cos\theta,$$

after which the binomial theorem gives

$$r_{1 \text{ or } 2}^{-3} \approx \left(r \pm \frac{d}{2}\cos\theta \right)^{-3} = r^{-3} \left(1 \pm \frac{d}{2r}\cos\theta \right)^{-3} \approx r^{-3} \left(1 \mp \frac{3d}{2r}\cos\theta \right).$$

Through this we approximate our expression for the magnetic field to

$$\mathbf{H(r)} \approx \frac{\rho_s a_d}{4\pi\mu_0 r^3} \left[\left(-\frac{1}{2}\mathbf{d} - \mathbf{r} \right) \left(1 - \frac{3d}{2r}\cos\theta \right) + \left(-\frac{1}{2}\mathbf{d} + \mathbf{r} \right) \left(1 + \frac{3d}{2r}\cos\theta \right) \right]$$

and further simplify as

$$\mathbf{H(r)} \approx \frac{\rho_s a_d d}{4\pi\mu_0 r^3} \left[-\hat{\mathbf{d}} + 3\cos\theta\hat{\mathbf{r}} \right]. \tag{2.1.4}$$

However, since $\hat{\mathbf{d}} \cdot \hat{\mathbf{r}} = \cos\theta$ and $M = \rho_s/\mu_0$ we can also write

$$\mathbf{H(r)} \approx \frac{MV}{4\pi r^3} \left[-\hat{\mathbf{d}} + 3\left(\hat{\mathbf{d}} \cdot \hat{\mathbf{r}} \right)\hat{\mathbf{r}} \right]. \tag{2.1.5}$$

Effect of Magnetic Fields on Dipoles Now that we've seen the field that a dipole produces, we also want to know the force and torque a dipole experiences when an external field is applied to it. To begin, we consider small dipole with axis $\mathbf{d}$ (along the direction of the magnetization). We then apply a magnetic field $\mathbf{H}_0$ to the dipole. We assume that the pole density is given by $\rho_s = \mu_0 M$, and is equal in magnitude and opposite in polarity on

13

opposite ends of the dipole with cross-sectional area a_d. Thus, the volume of the dipole is $\delta V = a_d d$ and the force on the dipole will be given by

$$-\mathbf{H}_0 \rho_s a_d + (\mathbf{H}_0 + \delta \mathbf{H}_0)\,\rho_s a_d = \delta \mathbf{H}_0 \rho_s a_d. \tag{2.1.6}$$

Where $\delta \mathbf{H}_0$ is the change in the applied field along the dipole's axis, and may therefore be given by $\delta \mathbf{H}_0 = (\mathbf{d} \cdot \nabla)\mathbf{H}_0 = (d/M)(\mathbf{M} \cdot \nabla)\mathbf{H}_0$. This first of these forms is useful because we may now define the dipole moment of a magnetic dipole $\mathbf{m} = \rho_s a_d \mathbf{d} = \mu_0 \mathbf{M} a_d d$ and rewrite the force as

$$(\mathbf{m} \cdot \nabla)\mathbf{H}_0 = \mu_0(\mathbf{M} \cdot \nabla)\mathbf{H}_0 \delta V. \tag{2.1.7}$$

This last equality now gives us the force density on a dipole

$$\text{force density} = \mu_0(\mathbf{M} \cdot \nabla)\mathbf{H}_0. \tag{2.1.8}$$

We now proceed to develop the torque on our dipole through similar arguments. We now assume $\delta \mathbf{H}_0 = \mathbf{0}$ and define the location of the south pole to be $\mathbf{r}_1$ and the north pole to be $\mathbf{r}_2$. We then have a torque

$$\delta \tau = \rho_s a_d\left(-\mathbf{r}_1 \times \mathbf{H}_0 + \mathbf{r}_2 \times \mathbf{H}_0\right) = \rho_s a_d \mathbf{d} \times \mathbf{H}_0, \tag{2.1.9}$$

where the last equality comes as a result of $\mathbf{r}_2 = \mathbf{r}_1 + \mathbf{d}$. Again, by virtue of $\rho_s a_d \mathbf{d} = \mu_0 \mathbf{M} \delta V$ we get a torque density on a dipole

$$\text{torque density} = \mu_0 \mathbf{M} \times \mathbf{H}_0. \tag{2.1.10}$$

Energy of Interaction Between Dipoles   Now that we've developed both the force on a dipole due to a magnetic field, and the magnetic field produced by a dipole, we may at last consider the energy associated with two dipoles interacting. We now define the $\mathbf{r}$ from our previous section on the field produced by a dipole to be the vector going from one of the dipoles to the other, and begin with the total force on a dipole from Eq. (2.1.7). We begin rewriting this force through the use of a vector identity as

$$(\mathbf{m} \cdot \nabla)\mathbf{H}_0 = \nabla(\mathbf{m} \cdot \mathbf{H}_0) - (\mathbf{H}_0 \cdot \nabla)\mathbf{m} - \mathbf{m} \times (\nabla \times \mathbf{H}_0) - \mathbf{H}_0 \times (\nabla \times \mathbf{m}). \tag{2.1.11}$$

For a lone dipole, we now have $\mathbf{m}$ constant, which causes two of the terms in the expansion to go to zero. In addition, Maxwell's equations tell us that when no electric fields or currents

are present $\nabla \times \mathbf{H}_0 = \mathbf{0}$. This leaves us with the force on the dipole

$$\mathbf{F} = \nabla(\mathbf{m} \cdot \mathbf{H}_0). \tag{2.1.12}$$

Therefore, since we have a force which can be written as the negative gradient of something else, that quantity is our energy

$$E = -(\mathbf{m} \cdot \mathbf{H}_0). \tag{2.1.13}$$

This is the energy of a dipole in an arbitrary magnetic field. We now return to Eq. (2.1.5) for the $\mathbf{H}_0$ in our case, as the magnetic field we are interested in is being produced by another dipole. This gives us an energy of

$$E = \mathbf{m}_1 \cdot \frac{M_2 V_2}{4\pi r^3} \left[\hat{\mathbf{d}}_2 - 3 \left(\hat{\mathbf{d}}_2 \cdot \hat{\mathbf{r}} \right) \hat{\mathbf{r}} \right], \tag{2.1.14}$$

after which we again exploit the definition of $\mathbf{m}$ to arrive at

$$E = \frac{1}{4\pi\mu_0 r^3} \left[\mathbf{m}_1 \cdot \mathbf{m}_2 - 3 \left(\mathbf{m}_1 \cdot \hat{\mathbf{r}} \right) \left(\mathbf{m}_2 \cdot \hat{\mathbf{r}} \right) \right]. \tag{2.1.15}$$

Therefore, we conclude that dipoles aligned along $\mathbf{r}$, the vector connecting their positions, is energetically favorable.

2.2 Ferrofluid Composition and Manufacture

Having established the basics of magnetic terminology and behavior, we pause the construction of governing relations to discuss first the basic makeup of ferrofluids. In general, the colloidal suspensions in ferrofluids are made up of particles with size varying between 3 and 15nm, which are then coated with a molecular layer of dispersant to prevent aggregation. The dispersant also ensures that while thermally induced Brownian motion keeps the particles in suspension, any collisions between particles are elastic.

The basic manufacturing process for ferrofluids with these characteristics is quite simple. Initially, an organic solvent (i.e. kerosene), the dispersant, and a powder of micron scale ferromagnetic material are all mixed together. These are then placed in a ball grinder for 500 to 1000 hours. This has the effect of making a number of the particles much smaller in size, and attaching the dispersant to them in the process. Next, the entire mixture is placed in a centrifuge, until any large conglomerations of particles that have formed have been sep-

arated. Lastly, additional solvent may be added, or some existing solvent removed, so ensure the final concentration is the desired one. The end result typically features concentrations of $\sim 10^{23}$ particles in every cubic meter of ferrofluid.

While this is the most straightforward manufacturing method, other methods also exist. Rosensweig (book) presents a number of such methods, and should be used as a more comprehensive guide than this paper, should the reader desire to attempt manufacture of ferrofluids. It is also important to distinguish the ferrofluids produced by these procedures from other "magnetic fluids" such as magnetorheological fluids, or those magnetically controllable fluids typically studied by magnetohydrodynamics. In typical magnetorheological fluid problems, the ferromagnetic particles in suspension are of micron scale rather than nanometer scale. This causes them to form chains when a strong magnetic field is applied, and the material as a bulk becomes effectively an elastic solid. In magnetohydrodynamics it is not ferromagnetic particles that are present in the liquid, but rather free charges, and forces produced by magnetic fields act perpendicularly. We distinguish ferrofluids from these cases by referring to materials which exhibit a direct inverse square force due to applied magnetic fields, and which feature sufficiently small particles to retain their fluidity in strong magnetic fields.

2.3   Stress Tensors in Ferrofluids

Before we can determine an expression for the stress tensor of a ferrofluid, we must first analyze what a stress tensor is. To aid us in this discussion, we begin with the Cauchy Stress Principle.

Theorem 2.3.1. *Cauchy Stress Principle* *Take ΔS to be a piece of the surface enclosing an arbitrary volume and let $\Delta \mathbf{f}$ be the force exerted on the material just inside that surface by things just outside it. Then the following limit is well-defined everywhere in the fluid:*

$$\lim_{\Delta S \to 0} \frac{\Delta \mathbf{f}}{\Delta S} = \frac{d\mathbf{f}}{dS} \equiv \mathbf{t}_n(\mathbf{r}), \qquad (2.3.1)$$

where we have defined a new quantity $\mathbf{t}_n(\mathbf{r})$ called the stress vector.

Proof. Recalling Eq. (2.4.8),

$$\frac{D}{Dt} \int_V (\rho \mathbf{v} + \mathbf{g})\, dV = \int_S \mathbf{t}_n dS + \int_V \rho \mathbf{b} dV,$$

we want to know what happens to these terms as our volume V shrinks to a point. Looking at the terms individually, we see that

$$\frac{D}{Dt}\int_V (\rho\mathbf{v} + \mathbf{g})\, dV \sim d^3 \quad \text{and} \quad \int_V \rho\mathbf{b}dV \sim d^3,$$

while

$$\int_S \mathbf{t}_n dS \sim d^2.$$

From this, we conclude that

$$\lim_{d\to 0}\frac{1}{d^2}\int_S \mathbf{t}_n dS = \mathbf{0}. \tag{2.3.2}$$

In other words, all stresses must be in local equilibrium, and we may write static force balance equations on infinitesimal volumes. As the Cauchy Stress Principle only states that the ratio of forces to areas approaches a definite limit as we approach a point, this is a restatement and the proof is complete. $\qquad\square$

Knowing that we can unambiguously characterize the stress at any given point, we now wish to find an expression that does this. To do so, we consider three mutually perpendicular planes at the point in question. For simplicity, they can be those planes whose normal vectors point along our coordinate axes. The Cauchy Stress Principle now tells us that we have a stress vector associated with each of these planes, each of which can be broken down into its three components:

$$\begin{aligned}
\mathbf{t}_x &= T_{xx}\hat{\mathbf{i}} + T_{xy}\hat{\mathbf{j}} + T_{xz}\hat{\mathbf{k}} \\
\mathbf{t}_y &= T_{yx}\hat{\mathbf{i}} + T_{yy}\hat{\mathbf{j}} + T_{yz}\hat{\mathbf{k}} \\
\mathbf{t}_z &= T_{zx}\hat{\mathbf{i}} + T_{zy}\hat{\mathbf{j}} + T_{zz}\hat{\mathbf{k}}.
\end{aligned} \tag{2.3.3}$$

From these equations, it is clear that we can construct a tensor T out of the dyadics

$$\mathsf{T} = \hat{\mathbf{i}}\mathbf{t}_x + \hat{\mathbf{j}}\mathbf{t}_y + \hat{\mathbf{k}}\mathbf{t}_z. \tag{2.3.4}$$

This allows to easily find the stress vector relative to any plane at any point simply through $\mathbf{t}_n = \mathbf{n}\cdot\mathsf{T}$, where $\mathbf{n}$ is the normal to the plane. Keeping in mind our original definition of this stress vector, and exploiting the divergence theorem, we have

$$\mathbf{F} = \oint_S \mathbf{t}_n dS = \oint_S \mathbf{n}\cdot\mathsf{T}dS = \int_V \nabla\cdot\mathsf{T}dV, \tag{2.3.5}$$

17

where **F** is the force on a body with surface S. This justifies our earlier use of $\nabla \cdot \mathsf{T}$ as a force density in our various balance equations.

We can now seek an expression for the specific form of the stress tensor in ferrofluids. In doing this we follow Rosensweig (book) completely, and the interested reader is directed to that text. The constitutive equations for ferrofluids will be presented with the stress tensor present in the following section, while the constitutive equations with explicit terms resulting therefrom will be presented in the following chapter, which we expect will make sufficient intuitive sense to leave the specifics to the text.

2.4   Principles of fluid mechanics

We present basic concepts in fluid mechanics required for the study of ferrohydrodynamics. In the study of fluid mechanics, one typically assumes the continuum hypothesis, conservation of mass, and conservation of momentum. Briefly, the continuum hypothesis states that quantities such as density, velocity, etc., are well defined infinitesimally; i.e., the molecular nature of the fluid is assumed to be of negligible impact, so that we are unconcerned with the discrete dynamics of the particles and instead view the fluid as a continuous body. For some fluids, such as gases with low density, this assumption is problematic, but it is generally very good for most liquids. One example of a liquid to which the continuum hypothesis does not apply very well is a polymer suspension in which the polymers can form chains.

As a consequence of the continuum hypothesis, full derivatives with respect to time appear somewhat differently than usual. Intuitively, because a fluid may have a velocity, quantities dependent on position and time change with respect to both time and transportation within the fluid. A simple application of the chain rule shows the formal relationship. Let $\psi = \psi(\mathbf{x}, t)$. Then

$$\frac{d\psi}{dt} = \frac{\partial \psi}{\partial t} + \frac{\partial x_i}{\partial t}\frac{\partial \psi}{\partial x_i} = \frac{\partial \psi}{\partial t} + \mathbf{v} \cdot \nabla \psi$$

For the sake of clarity, it is common to label $\frac{d}{dt}$ as $\frac{D}{Dt}$, and call the operator the *substantive derivative* (or sometimes the *material derivative*):

$$\frac{D}{Dt} = \frac{\partial}{\partial t} + \mathbf{v} \cdot \nabla \tag{2.4.1}$$

However, in our paper we will not follow this convention, as it really is just another way of writing the full derivative and can get confusing at times.

Suppose $\mathbf{x_0}$ is a fixed point in $\mathbb{R}^3$ and $\mathbf{x} = \phi(\mathbf{x_0}, \mathbf{t})$ is the position of an element of fluid starting at $\mathbf{x_0}$ after a time t. We let J denote the determinant of the Jacobian matrix of this transformation; $J = \det(\frac{\partial x^i}{\partial x_0^j})$. We'll need the following lemma:

Lemma 2.4.1. $\frac{dJ}{dt} = J\nabla \cdot \mathbf{v}$.

Proof. Note that the Jacobian can be written $J = \frac{\partial x^i}{\partial x_o^j} M_{ij}$, where M_{ij} is the cofactor of $\frac{\partial x^i}{\partial x_0^j}$. Direct computation gives

$$\frac{dJ}{dt} = \frac{\partial v^i}{\partial x_o^j} M_{ij} = \frac{\partial v^i}{\partial x^i} \frac{\partial x^i}{\partial x_o^j} M_{ij} = J \frac{\partial v^i}{\partial x^i}.$$

$\square$

The following theorem is fundamental to fluid mechanics:

Theorem 2.4.2. (*Reynolds transport theorem*) *Let* $V = V(t)$ *be the volume of an element of fluid that deforms with time,* S *its surface, and* $\mathbf{n}$ *an outward normal unit vector to the surface. For any function* $\psi = \psi(\mathbf{x}, t)$, *we have*

$$\frac{d}{dt} \int_V \psi dV = \int_V \frac{\partial \psi}{\partial t} dV + \oint_S (\mathbf{n} \cdot \mathbf{v}\psi) dS \qquad (2.4.2)$$

Proof. Let V_0 indicate $V(0)$. Then

$$\frac{d}{dt} \int_V \psi dV = \frac{d}{dt} \int_{V_0} \psi J dV_0$$

Because the volume of integration is constant, we may bring the differential operator inside the integral, so that

$$\frac{d}{dt} \int_V \psi dV = \int_{V_0} \frac{d}{dt}(\psi J) dV_0.$$

We apply the product rule, and the lemma we just proved:

$$\frac{d}{dt} \int_V \psi dV = \int_{V_0} \left(J\frac{d\psi}{dt} + \psi \frac{dJ}{dt} \right) dV_0 = \int_{V_0} \left(J\frac{d\psi}{dt} + \psi J\nabla \cdot \mathbf{v} \right) dV_0.$$

19

Now, transforming the volume of integration back to $V(t)$ and computing the substantive derivative of ψ gives

$$\frac{d}{dt}\int_V \psi dV = \int_V \left(\frac{\partial \psi}{\partial t} + \mathbf{v}\cdot\nabla\psi + \psi\nabla\cdot\mathbf{v}\right)dV.$$

Finally, we note that $\mathbf{v}\cdot\nabla\psi + \psi\nabla\cdot\mathbf{v} = \nabla\cdot(\mathbf{v}\psi)$ and apply the divergence theorem to give

$$\frac{d}{dt}\int_V \psi dV = \int_V \left(\frac{\partial \psi}{\partial t} + \nabla\cdot(\mathbf{v}\psi)\right)dV = \int_V \frac{\partial \psi}{\partial t}dV + \oint_S (\mathbf{n}\cdot\mathbf{v}\psi)dV. \qquad (2.4.3)$$

$\square$

For the following sections, we essentially follow [Rosensweig, "Basic Equations for Magnetic Fluids," S. Odenbach, Ferrofluids: Magnetically Controllable Fluids and their Applications].

2.4.1 Conservation of mass

Consider a volume V of fluid with surface S and constant mass, with mass density given by $\rho = \rho(\mathbf{x}, t)$. The expression of conservation of mass is given by

$$\frac{d}{dt}\int_V \rho dV = 0. \qquad (2.4.4)$$

One can apply the Reynolds transport theorem (2.4.3) to give

$$\int_V \left(\frac{\partial \rho}{\partial t} + \nabla\cdot(\rho\mathbf{v})\right)dV = 0.$$

Since this must work over any volume, we have

$$\frac{\partial \rho}{\partial t} + \nabla\cdot(\rho\mathbf{v}) = 0. \qquad (2.4.5)$$

This is known as the *continuity equation*. Alternatively, one may write

$$\frac{1}{\rho}\frac{d\rho}{dt} = -\nabla\cdot\mathbf{v}. \qquad (2.4.6)$$

Using the continuity equation, we obtain a corollary of the Reynolds transport theorem:

20

$$\frac{d}{dt} \int_V \rho\psi dV = \int_V \left(\frac{\partial}{\partial t}(\rho\psi) + \nabla \cdot (\mathbf{v}\rho\psi) \right) dV$$

$$= \int_V \left(\rho\frac{\partial\psi}{\partial t} + \psi\frac{\partial\rho}{\partial t} + \psi\nabla \cdot (\mathbf{v}\rho) + \rho\nabla \cdot (\mathbf{v}\psi) \right) dV$$

$$= \int_V \left(\rho\frac{\partial\psi}{\partial t} + \rho\nabla \cdot (\mathbf{v}\psi) \right) dV$$

$$\frac{d}{dt} \int_V \rho\psi dV = \int_V \rho\frac{d\psi}{dt} dV \tag{2.4.7}$$

2.4.2 Linear momentum conservation

To express the conservation of momentum, we consider the substantive derivative of the momentum of the volume and equate it with the sum of surface and body forces. We let $\mathbf{g}$ be the electromagnetic momentum density vector, $\mathbf{t}_n$ the surface stress vector, and $\mathbf{b}$ the body force vector. We then have

$$\frac{d}{dt} \int_V (\rho\mathbf{v} + \mathbf{g}) \, dV = \int_S \mathbf{t}_n dS + \int_V \rho\mathbf{b} dV. \tag{2.4.8}$$

Applying the corollary Reynolds transport theorem (2.4.7) gives

$$\frac{d}{dt} \int_V (\rho\mathbf{v}) dV = \int_V \rho\frac{d\mathbf{v}}{dt} dV,$$

and applying (2.4.3) gives

$$\frac{d}{dt} \int_V \mathbf{g} dV = \int_V \left(\frac{\partial\mathbf{g}}{\partial t} + \nabla \cdot (\mathbf{v}\mathbf{g}) \right) dV.$$

Finally, Cauchy's theorem of fluid stresses gives that $\mathbf{t}_n = \mathbf{n} \cdot \mathsf{T}$, where $\mathbf{n}$ is a normal vector to the surface and T is the stress tensor of the fluid. We can then write

$$\int_S \mathsf{T}_n dS = \int_s \mathbf{n} \cdot \mathsf{T} dS = \int_V \nabla \cdot \mathsf{T} dV.$$

Combining these results and invoking the arbitrary nature of the volume of integration we have

$$\rho\frac{d\mathbf{v}}{dt} + \frac{\partial\mathbf{g}}{\partial t} = \nabla \cdot \mathsf{T}' + \rho\mathbf{b}, \tag{2.4.9}$$

where

$$\mathsf{T}' = \mathsf{T} - \mathbf{vg}. \tag{2.4.10}$$

A more detailed description of T will be dealt with later in the paper.

2.4.3 Angular momentum conservation

Similarly, we can find a balance equation for angular momentum by equating the rate of change of angular momentum with the sum of all the torques on the body of fluid. However, we must also take into consideration the individual spins of the ferromagnetic particles suspended in the fluid, along with the surface and volume coupling due to transmission of spin angular momentum through the fluid. Let $\mathbf{r_0}$ be the position vector of a fluid element with respect to a fixed location, $\mathbf{s}$ the spin angular momentum density, λ_n the surface couple density, and $\mathbf{l}$ the volume couple density. Then

$$\frac{d}{dt} \int_V \left[\mathbf{r} \times (\rho \mathbf{v} + \mathbf{g}) + \rho \mathbf{s} \right] dV = \int_S \left(\mathbf{r} \times \mathsf{T}_n + \lambda_n \right) dS + \int_V \left(\mathbf{r} \times \rho \mathbf{b} + \rho \mathbf{l} \right) dV \tag{2.4.11}$$

.

Using (2.4.7), along with noting that $\mathbf{v} = \frac{d\mathbf{r}}{dt}$, we have

$$\frac{d}{dt} \int_V \mathbf{r} \times \rho \mathbf{v} dV = \int_V \left(\mathbf{r} \times \rho \frac{d\mathbf{v}}{dt} \right) dV. \tag{2.4.12}$$

Similarly,

$$\frac{d}{dt} \int_V \mathbf{r} \times \mathbf{g} dV = \int_V \left(\mathbf{v} \times \mathbf{g} + \mathbf{r} \times \left[\frac{\partial \mathbf{g}}{\partial t} + \nabla \cdot (\mathbf{vg}) \right] \right) dV. \tag{2.4.13}$$

Again noting that $\mathbf{t}_n = \mathbf{n} \cdot \mathsf{T}$ applying the divergence theorem gives

$$\int_S \left(\mathbf{r} \times \mathbf{t}_n \right) dS = - \int_V \nabla \cdot (\mathsf{T} \times \mathbf{r}) dV. \tag{2.4.14}$$

We apply the identity $-\nabla \cdot (\mathsf{T} \times \mathbf{r}) = \mathbf{r} \times (\nabla \cdot \mathsf{T}) - \epsilon : \mathsf{T}$, where ϵ is the Levi-Civita third-rank permutation tensor. This yields

$$\int_S \left(\mathbf{r} \times \mathbf{t}_n \right) dS = - \int_V \mathbf{r} \times (\nabla \cdot \mathsf{T}) - \epsilon : \mathsf{T} dV. \tag{2.4.15}$$

Similarly to the surface stress vector, the couple stress vector satisfies $\lambda_n = \mathbf{n} \cdot \Lambda$, where

22

Λ is the couple stress tensor. So, using this and the divergence theorem,

$$\int_S \lambda_n dS = \int_V \nabla \cdot \Lambda dV. \tag{2.4.16}$$

Combining (2.4.12), (2.4.13), (2.4.14), (2.4.15), and (2.4.16) into (2.4.11) gives us

$$\int_V \left[\rho \frac{d\mathbf{s}}{dt} + \mathbf{r} \times \left(\rho \frac{d\mathbf{v}}{dt} + \frac{\partial \mathbf{g}}{\partial t} - \nabla \cdot (\mathsf{T} - \mathbf{v}\mathbf{g}) - \rho \mathbf{b} \right) \right] dV = \int_V \left[\rho \mathbf{l} + \nabla \cdot \Lambda - \epsilon : (\mathsf{T} - \mathbf{v}\mathbf{g}) \right] dV. \tag{2.4.17}$$

The second term in the first integral drops out by virtue of (2.4.9), and we reuse our definition T'. Invoking the arbitrariness of the volume of integration gives:

$$\rho \frac{d\mathbf{s}}{dt} = \rho \mathbf{l} + \nabla \cdot \Lambda - \epsilon : \mathsf{T}. \tag{2.4.18}$$

2.4.4 Energy conservation and thermodynamics

We start with a few remarks on energetics of electromagnetic interactions. The density of electromagnetic energy flux is given by the Poynting vector $\mathbf{E}' \times \mathbf{H}'$, where $\mathbf{E}'$ and $\mathbf{H}'$ are, respectively, the electric and magnetic fields observed in a moving coordinate system; e.g., moving with the fluid. For non-relativistic speeds, $\mathbf{E}' = \mathbf{E} + \mathbf{v} \times \mathbf{B}$, with $\mathbf{E}$ the electric field observed in a stationary coordinate system, $\mathbf{v}$ the velocity, and $\mathbf{B}$ the magnetic induction. Similarly, $\mathbf{H}' = \mathbf{H} - \mathbf{v} \times \mathbf{D}$, with $\mathbf{H}$ the magnetic field observed in a stationary coordinate system, and $\mathbf{D}$ the electric displacement. Here,

$$\mathbf{D} = \epsilon_0 \mathbf{E} + \mathbf{P}, \tag{2.4.19}$$
$$\mathbf{B} = \mu_0 \left(\mathbf{H} + \mathbf{M} \right), \tag{2.4.20}$$

with $\mathbf{P}$ the electric polarization of the fluid and $\mathbf{M}$ the magnetization of the fluid.

Now, let u be the internal energy per unit mass of the fluid, I be the moment of inertia per unit mass of the particles, Ω the magnitude of angular velocity of the particles, and $\mathbf{q}$ the heat flux vector. Then the balance of energy for a ferrofluid system is expressible by

$$\frac{d}{dt} \int_V \rho \left(u + \frac{v^2}{2} + \frac{I\Omega^2}{2} \right) dV =$$

$$\int_S \mathbf{t}_n \cdot \mathbf{v} dS + \int_V \rho \mathbf{b} \cdot \mathbf{v} dV + \int_S \lambda_n \cdot \mathbf{v} + \int_V \rho \mathbf{l} \cdot \mathbf{\Omega} dV \qquad (2.4.21)$$

$$- \int_S \mathbf{n} \cdot \mathbf{q} dS - \int_S \mathbf{n} \cdot (\mathbf{E}' \times \mathbf{H}') \, dS.$$

As usual, we apply the Reynolds transport theorem to the left side of (2.4.21), transform surface integrals into volume integrals with the divergence theorem and Cauchy's stress theorem (Thm. 2.3.1), and note that the volume of integration is arbitrary. In addition, we use the vector identity $\nabla \cdot (\mathsf{A} \cdot \mathbf{b}) = (\nabla \cdot \mathsf{A}) \cdot \mathbf{b} + \mathsf{A}^{\mathrm{T}} : \nabla \mathbf{b}$ to obtain

$$\rho \frac{du}{dt} + \left(\rho \frac{d\mathbf{v}}{dt} - \nabla \cdot \mathsf{T}' - \rho \mathbf{b} \right) \cdot \mathbf{v} + \left(\rho I \frac{d\mathbf{\Omega}}{dt} - \nabla \cdot \mathbf{\Lambda} - \rho \mathbf{l} \right) \cdot \mathbf{\Omega}$$

$$= \mathsf{T}'^{\mathrm{T}} : \nabla \mathbf{v} + \mathbf{\Lambda}^{\mathrm{T}} : \nabla \mathbf{\Omega} - \nabla \cdot (\mathbf{E}' \times \mathbf{H}') - \nabla \cdot \mathbf{q}. \qquad (2.4.22)$$

It is convenient to view the electromagnetic energy flux from stationary coordinates. To do so, we use $\mathbf{E}' = \mathbf{E} + \mathbf{v} \times \mathbf{B}$ and $\mathbf{H}' = \mathbf{H} - \mathbf{v} \times \mathbf{D}$. Then, after some extremely messy elementary algebra,

$$-\nabla \cdot (\mathbf{E}' \times \mathbf{H}') = -\nabla \cdot (\mathbf{E} \times \mathbf{H}) - [\mathbf{E} \cdot \{\nabla \times (\mathbf{v} \times \mathbf{D})\} + \mathbf{H} \cdot \{\nabla \times (\mathbf{v} \times \mathbf{B})\}]$$

$$+ [(\nabla \times \mathbf{E}) \cdot (\nabla \times \mathbf{D}) + (\nabla \times \mathbf{H}) \cdot (\nabla \times \mathbf{B})] + \nabla \cdot [(\mathbf{v} \times \mathbf{B}) \times (\mathbf{v} \times \mathbf{D})].$$

Now, we can use Maxwell's equations to transform the third term of this expression. Note that $\frac{\partial \mathbf{B}}{\partial t} = \nabla \times \mathbf{E}$, and $\frac{\partial \mathbf{D}}{\partial t} = \nabla \times \mathbf{H} - \mathbf{j}$, with $\mathbf{j}$ the current density. We then have

$$[(\nabla \times \mathbf{E}) \cdot (\nabla \times \mathbf{D}) + (\nabla \times \mathbf{H}) \cdot (\nabla \times \mathbf{B})]$$

$$= -\frac{\partial \mathbf{g}}{\partial t} \cdot \mathbf{v} + \mathbf{j}' \cdot (\mathbf{v} \times \mathbf{B}),$$

where $\mathbf{j}' = \mathbf{j} - \rho_e \mathbf{v}$ is the current density measured moving with the fluid, and

$$\mathbf{g} = \mathbf{D} \times \mathbf{B} \qquad (2.4.23)$$

24

is the electromagnetic energy density. Note, of course, that the $\rho_e \mathbf{v}$ term is included for completion, as it vanishes in the scalar product with $\mathbf{v} \times \mathbf{B}$.

Using vector identities and the definition of $\mathbf{g}$, we can also find

$$
\begin{aligned}
\nabla \cdot [(\mathbf{v} \times \mathbf{B}) \times (\mathbf{v} \times \mathbf{D})] &= \mathbf{v} \cdot (\mathbf{B} \times \mathbf{D}) \nabla \cdot \mathbf{v} + \mathbf{v} \cdot \nabla (\mathbf{v} \cdot \mathbf{B} \times \mathbf{D}) \\
&= -(\mathbf{v} \cdot \mathbf{g}) \nabla \cdot \mathbf{v} - \mathbf{v} \cdot (\mathbf{v} \cdot \nabla \mathbf{g}) - \mathbf{v} \cdot (\mathbf{g} \cdot \nabla \mathbf{v}) \\
&= -[\nabla \cdot (\mathbf{v}\mathbf{g})] \cdot \mathbf{v} - (\mathbf{v}\mathbf{g} : \nabla \mathbf{v}).
\end{aligned}
$$

So,

$$
\begin{aligned}
-\nabla \cdot (\mathbf{E}' \times \mathbf{H}') &= -\nabla \cdot (\mathbf{E} \times \mathbf{H}) - [\mathbf{E} \cdot \{\nabla \times (\mathbf{v} \times \mathbf{D})\} + \mathbf{H} \cdot \{\nabla \times (\mathbf{v} \times \mathbf{B})\}] \\
&+ [(\nabla \times \mathbf{E}) \cdot (\nabla \times \mathbf{D}) + (\nabla \times \mathbf{H}) \cdot (\nabla \times \mathbf{B})] - [\nabla \cdot (\mathbf{v}\mathbf{g})] \cdot \mathbf{v} - (\mathbf{v}\mathbf{g} : \nabla \mathbf{v}). \quad (2.4.24)
\end{aligned}
$$

Now, the basic identity for the vector triple product and Maxwell's equations (specifically, $\nabla \cdot \mathbf{B} = 0$ and $\nabla \cdot \mathbf{D} = \rho_e$) tells us

$$
\nabla \times (\mathbf{v} \times \mathbf{B}) = (\mathbf{B} \cdot \nabla)\mathbf{v} - (\mathbf{v} \cdot \nabla)\mathbf{B} - (\nabla \cdot \mathbf{v})\mathbf{B},
$$

and

$$
\nabla \times (\mathbf{v} \times \mathbf{D}) = (\mathbf{D} \cdot \nabla)\mathbf{v} - (\mathbf{v} \cdot \nabla)\mathbf{D} - (\nabla \cdot \mathbf{v})\mathbf{D} + \rho_e \mathbf{v}.
$$

Note also that by Maxwell's equations,

$$
\frac{d\mathbf{B}}{dt} = \nabla \times \mathbf{E} + (\mathbf{v} \cdot \nabla)\mathbf{B} = \nabla \times \mathbf{E} + (\mathbf{B} \cdot \nabla)\mathbf{v} - (\nabla \cdot \mathbf{v})\mathbf{B} - \nabla \times (\mathbf{v} \times \mathbf{B}),
$$

and

$$
\frac{d\mathbf{D}}{dt} = \nabla \times \mathbf{H} - \mathbf{j} + (\mathbf{v} \cdot \nabla)\mathbf{D} = \nabla \times \mathbf{H} - \mathbf{j} - (\nabla \cdot \mathbf{v})\mathbf{D} + \rho_e \mathbf{v} + (\mathbf{D} \cdot \nabla)\mathbf{v} - \nabla \times (\mathbf{v} \times \mathbf{D}).
$$

With these expressions, we can easily obtain the divergence of the Poynting vector by taking the dot product of the preceding two equations with $\mathbf{H}$ and $\mathbf{E}$, respectively, and rearranging the terms:

$$\nabla \cdot (\mathbf{E} \times \mathbf{H}) = -\mathbf{j}^* \cdot \mathbf{E} - \mathbf{E} \cdot \frac{d\mathbf{D}}{dt} - \mathbf{H} \cdot \frac{d\mathbf{B}}{dt}$$
$$+ \left[\mathbf{ED} + \mathbf{HB} - (\mathbf{D} \cdot \mathbf{E} + \mathbf{B} \cdot \mathbf{H})\mathsf{I} \right] : \nabla \mathbf{v} \qquad (2.4.25)$$
$$- \left[\mathbf{E} \cdot \{ \nabla \times (\mathbf{v} \times \mathbf{D}) \} + \mathbf{H} \cdot \{ \nabla \times (\mathbf{v} \times \mathbf{B}) \} \right].$$

We combine linear and angular momentum balance equations into (2.4.22) to obtain

$$\rho \frac{du}{dt} - \frac{\partial \mathbf{g}}{\partial t} \cdot \mathbf{v} + \mathsf{T} : \epsilon \cdot \boldsymbol{\Omega}$$
$$= \mathsf{T}'^{\mathrm{T}} : \nabla \mathbf{v} + \boldsymbol{\Lambda}^{\mathrm{T}} : \nabla \boldsymbol{\Omega} - \nabla \cdot (\mathbf{E}' \times \mathbf{H}') - \nabla \cdot \mathbf{q}. \qquad (2.4.26)$$

Using (2.4.26) along with (2.4.24) and (2.4.25), along with a few routine algebraic manipulations, we obtain a differential law of energy conservation:

$$\rho \frac{du}{dt} = \mathsf{T}'^{\mathrm{T}} : \nabla \mathbf{v} + \boldsymbol{\Lambda}^{\mathrm{T}} : \nabla \boldsymbol{\Omega} - \mathsf{T} : \epsilon \cdot \boldsymbol{\Omega}$$
$$- \left[\mathbf{ED} + \mathbf{HB} - (\mathbf{D} \cdot \mathbf{E} + \mathbf{B} \cdot \mathbf{H})\mathsf{I} \right] : \nabla \mathbf{v} \qquad (2.4.27)$$
$$+ \mathbf{E} \cdot \frac{d\mathbf{P}}{dt} + \mathbf{H} \cdot \frac{d\mathbf{M}}{dt} + \mathbf{j}^* \cdot \mathbf{E}^* - \nabla \cdot \mathbf{q}.$$

It is sometimes convenient to look at the internal energy of the fluid itself, as (2.4.27) describes the dynamics of the energy of the entire system, including the electromagnetic field energy. We let u_f be the energy, defined by subtracting away the field energy:

$$u_f \equiv u - \frac{\epsilon_0 E^2}{2\rho} - \frac{\mu_0 H^2}{2\rho}. \qquad (2.4.28)$$

The differential law here is easily seen to be

$$\rho \frac{du_f}{dt} = \mathsf{T}'^{\mathrm{T}} : \nabla \mathbf{v} + \mathbf{\Lambda}^{\mathrm{T}} : \nabla \mathbf{\Omega} - \mathsf{T} : \epsilon \cdot \mathbf{\Omega}$$
$$- [\mathbf{ED} + \mathbf{HB} - (\mathbf{D} \cdot \mathbf{E} + \mathbf{B} \cdot \mathbf{H})\mathsf{I}] : \nabla \mathbf{v} \qquad (2.4.29)$$
$$+ \mathbf{E} \cdot \frac{d\mathbf{P}}{dt} + \mathbf{H} \cdot \frac{d\mathbf{M}}{dt} + \mathbf{j}^* \cdot \mathbf{E}^* - \nabla \cdot \mathbf{q}.$$
$$- \frac{d}{dt} \left(\frac{\epsilon_0 E^2}{2} - \frac{\mu_0 H^2}{2} \right).$$

In the discussion which follows, we will consider $\mathbf{E}$ to be negligible, and will properly motivate this decision when we begin further discussion. However, we will need a fully developed theory of the magnetization of the fluid, so we turn to that now.

2.5 Magnetization equation

Here we derive a simple phenomenological magnetization equation from basic thermodynamics. We assume an equilibrium magnetization $\mathbf{M_0}$ and investigate small deviations from this equilibrium. In near-equilibrium theory, the relaxation of these deviations towards equilibrium is a simple exponential dependence.

Following Landau, we assume that the time rate of change of $\mathbf{M}$ is proportional to the partial derivative of the Gibbs free energy, G, with respect to $\mathbf{M}$:

$$\frac{d\mathbf{M}}{dt} = -\gamma \frac{\partial G}{\partial \mathbf{M}}, \qquad (2.5.1)$$

where $\gamma > 0$ and $\frac{\partial G}{\partial \mathbf{M}} = \left(\frac{\partial G}{\partial M_1}, \frac{\partial G}{\partial M_2}, \frac{\partial G}{\partial M_3} \right)$. By a simple application of the chain rule,

$$\frac{dG}{dt} = \frac{\partial G}{\partial \mathbf{M}} \cdot \frac{d\mathbf{M}}{dt} = -\gamma \left(\frac{\partial G}{\partial \mathbf{M}} \right)^2, \qquad (2.5.2)$$

which simply describes how the free energy decreases when the system moves to equilibrium. In weak nonequilibrium conditions, we can use a linear Taylor series expansion:

$$\frac{\partial G}{\partial \mathbf{M}} \approx \left(\frac{\partial G}{\partial \mathbf{M}} \right)_{\mathbf{M}=\mathbf{M_0}} + (\mathbf{M} - \mathbf{M_0}) \left(\frac{\partial^2 G}{\partial \mathbf{M}^2} \right)_{\mathbf{M}=\mathbf{M_0}}$$

Applying this linearization to (2.5.1) and (2.5.2) gives

$$\frac{dG}{dt} = -\frac{(\mathbf{M} - \mathbf{M_0})^2}{\gamma\tau^2} \tag{2.5.3}$$

where $\tau = \left(\gamma\left(\frac{\partial^2 G}{\partial \mathbf{M^2}}\right)_{\mathbf{M=M_0}}\right)^{-1}$ is the Brownian time of rotational particle diffusion. We can also write this purely in terms of the magnetization:

$$\frac{d'\mathbf{M}}{dt} = -\frac{1}{\tau}(\mathbf{M} - \mathbf{M_0}), \tag{2.5.4}$$

where we introduce the notation $\frac{d'}{dt}$ to note that the equation governs the magnetization only in the local frame. To take care of this, we note that the ferromagnetic particles are rotating with angular velocity given by

$$\omega = \frac{1}{6\eta\phi}\mathbf{M} \times \mathbf{H} + \mathbf{\Omega}$$

By the simple kinematic expression $\frac{d\mathbf{Y}}{dt} = \omega \times \mathbf{Y} + \frac{d'\mathbf{Y}}{dt}$ for any vector quantity $\mathbf{Y}$, where the primed derivative is taken inside a frame rotating at angular velocity ω, we have

$$\frac{d\mathbf{M}}{dt} = \mathbf{\Omega} \times \mathbf{M} - \frac{1}{\tau}(\mathbf{M} - \mathbf{M_0}) - \frac{1}{6\eta\phi}\mathbf{M} \times (\mathbf{M} \times \mathbf{H}). \tag{2.5.5}$$

Fortunately, for most physically reasonable situations (and for the physics of our problem) displacement from equilibrium is small enough so that the initial linearization is a very good approximation.

For completeness, we mention that often one uses a fairly standard collinearity approximation $\mathbf{M} = \chi\mathbf{H}$, with χ the magnetic susceptibility, however, our analysis will eschew this assumption.

2.6 Experimental Considerations

With these very general expressions in mind, we now seek to apply them to a specific experimental setup. The situation we consider is that of a ferrofluid in a Hele-Shaw cell under a very particular applied magnetic field. Before the details of the field are discussed, a brief explanation of Hele-Shaw cells is in order.

A Hele-Shaw cell is two plates of glass placed a small, fixed distance apart from one another. This cell thickness is typically on the order of ~ 1 mm. This results in an essentially two dimensional problem. When the ferrofluid is placed in the cell, another fluid is added as a buffer so that the ferrofluid does not come into direct contact with the air. This buffer fluid is usually ignorable, but will be explicitly mentioned when looking at boundary conditions later.

In addition to the dimensionality, the other facet we gain from the experimental setup is that no electric fields are applied. This means that the only electric fields present are those that result from induction when the applied magnetic field changes in time. As these are scaled by a factor of c^2 we assume electric fields, along with free currents to be negligible[1]. We add to this the assumption that the cell is sufficiently small to be of uniform temperature, and arrive at a small set of simplifying equations:

$$
\begin{aligned}
\mathbf{E}, \mathbf{E}', \mathbf{D} &= \mathbf{0}, \\
\rho_e &= 0, \\
\mathbf{j}, \mathbf{j}' &= \mathbf{0}, \\
\nabla \cdot \mathbf{q} &= 0, \\
\Rightarrow g &= 0, \\
\Rightarrow \mathsf{T} &= \mathsf{T}'.
\end{aligned}
\tag{2.6.1}
$$

These now allow us to take the explicit form of the stress tensor and develop the model for Hele-Shaw flow. The final consideration is the applied magnetic field. We look at the case of a constant axial magnetic field perpendicular to the plane of the Hele-Shaw cell, along with a uniform transverse magnetic field within the cell, the direction of which rotates in time. This is the setup used by Zahn et. al. [17], and the configuration we wish to analyze. The magnetic field is more explicitly dealt with in Chapter 4

---

[1]The conclusion on free currents arises due to the lack of free electric charge.

Chapter 3

Model

In this chapter we shall derive a model for the flow of the ferrofluid through the Hele-Shaw cell. The basic idea is that the fluid moves quite slowly, so that its velocity is constant and so that viscous effects dominate the fluid (the low Reynolds number limit). We will consider this principle and use it to remove inertial terms from the Navier-Stokes equation, and use the two-dimensional geometry to arrive at a simple governing equation.

We start with the Navier-Stokes equation for ferrofluids:

$$\rho \frac{d\mathbf{v}}{dt} = -\nabla p + \mu_0 \nabla \mathbf{H} \cdot \mathbf{M} + 2\xi \nabla \times \mathbf{\Omega} + (\lambda + \eta - \xi)\nabla(\nabla \cdot \mathbf{v}) + (\eta + \xi)\nabla^2 \mathbf{v}, \qquad (3.0.1)$$

and the governing equation for the spin velocity of the magnetic particles:

$$I\frac{d\mathbf{\Omega}}{dt} = \mu_0 \mathbf{M} \times \mathbf{H} + 4\xi(\omega - \mathbf{\Omega}) + (\lambda' + \eta')\nabla(\nabla \cdot \mathbf{\Omega}) + \eta'\nabla^2\mathbf{\Omega}. \qquad (3.0.2)$$

According to Zahn et al. [21], experiments corroborate the following assumptions:

- The flow is incompressible, so that $\nabla \cdot \mathbf{v} = 0$ everywhere in the fluid. We can also make the even stronger assumption that ρ is a constant.

- The flow is steady, so that it is dominated by viscous effects; consequently, $\frac{d\mathbf{v}}{dt} \approx \mathbf{0}$, and $\frac{d\mathbf{\Omega}}{dt} \approx \mathbf{0}$.

- The two-dimensional geometry of the experiment implies that $\nabla \cdot \mathbf{\Omega} = 0$.

- By dimensional analysis arguments, $\eta' \sim \eta l^2 \phi^2$, with l the distance between magnetic particles and ϕ the volume fraction of the particles. As in ferrofluids l is on the order of nanometers and $\phi \approx 0.01$, we assume η' is negligible.

Combining these assumptions with Eqs. (3.0.1) and (3.0.2) give the following approximations:

$$\mathbf{0} = -\nabla p + \mu_0 \nabla \mathbf{H} \cdot \mathbf{M} + \frac{\mu_0}{2} \nabla \times (\mathbf{M} \times \mathbf{H}) + \eta \nabla^2 \mathbf{v} \tag{3.0.3}$$

$$\mathbf{\Omega} = \frac{\mu_0 \mathbf{M} \times \mathbf{H}}{4\xi} + \frac{1}{2} \nabla \times \mathbf{v} \tag{3.0.4}$$

From (3.0.3) we can derive a simplified equation for the dynamics of the flow known as *Darcy's law* by averaging the velocity over the z direction. We first need three additional assumptions. The first two are easily justifiable, the third requires a bit more work:

- ∇p, $\mathbf{M}$ and $\mathbf{H}$ are uniform along the z direction through the cell.

- The system has no-slip boundary conditions at $z = h/2$ and $z = -h/2$; i.e., the velocity is zero there.

- $\dfrac{\partial^2 \mathbf{v}}{\partial x^2}$ and $\dfrac{\partial^2 \mathbf{v}}{\partial y^2}$ are both negligible.

The third assumption is rationalized by considering the flow well before the onset of instabilities. As finger and labyrinth formation has not yet occurred, we expect the flow to be relatively spatially uniform throughout the cell; the viscosity-dominated nature of the flow lends credence to this expectation. Furthermore, our hypothesis is that the instabilities we are looking for are primarily due to the influence of magnetization on the spin velocity, so we do not expect these terms to be important.

We then have that (3.0.3) reduces to

$$-\eta \frac{\partial^2 \mathbf{v}}{\partial z^2} = -\nabla p + \mu_0 \nabla \mathbf{H} \cdot \mathbf{M} + \frac{\mu_0}{2} \nabla \times (\mathbf{M} \times \mathbf{H}). \tag{3.0.5}$$

Integrating twice from $-h/2$ to $h/2$ gives

$$\mathbf{v} = \frac{-1}{\eta} \left[-\nabla p + \mu_0 \nabla \mathbf{H} \cdot \mathbf{M} + \frac{\mu_0}{2} \nabla \times (\mathbf{M} \times \mathbf{H}) \right] \left(z^2 - \frac{h^2}{4} \right). \tag{3.0.6}$$

We now average $\mathbf{v}$ over z by integrating from $-h/2$ to $h/2$ and dividing by h:

$$\bar{\mathbf{v}} = \frac{1}{h} \int_{-h/2}^{h/2} \frac{-1}{\eta} \left[-\nabla p + \mu_0 \nabla \mathbf{H} \cdot \mathbf{M} + \frac{\mu_0}{2} \nabla \times (\mathbf{M} \times \mathbf{H}) \right] \left(z^2 - \frac{h^2}{4} \right) dz \tag{3.0.7}$$

We then have

$$\mathbf{v} = \frac{h^2}{12\eta} \left[-\nabla p + \mu_0 \nabla \mathbf{H} \cdot \mathbf{M} + \frac{\mu_0}{2} \nabla \times (\mathbf{M} \times \mathbf{H}) \right]. \tag{3.0.8}$$

Note that, physically, this is simply stating that resistance terms are great enough so that the velocity is proportional to the force. Now, since the fluid is incompressible, taking the divergence of both sides of (3.0.8) gives

$$\nabla^2 p = \mu_0 \nabla \cdot (\nabla \mathbf{H} \cdot \mathbf{M}), \tag{3.0.9}$$

so the pressure satisfies a Poisson equation. The boundary values are to be specified later.

3.1 Discussion of the Model

There is still some work to do to ensure that our model accurately describes the phenomenon in question. We have so far only considered ferrofluid properties such as pressure and magnetization, but the shape of the deformed droplet is also quite important, as is the requirement of continuity. Mathematically, this changes the pressure Poisson equation (3.0.9) to a moving boundary problem, which is of an entirely different character. This free boundary heavily complicates the otherwise simple elliptic pressure Poisson equation.

One other aspect of the dynamics that we have not yet discussed is the surrounding fluid in the Hele-Shaw cell. Recall that the ferrofluid is surrounded by another non-magnetic fluid. This fluid obeys its own form of Darcy's law, with the dynamics described as being proportional to the gradient of its own pressure. These two fluids are coupled by the fact that their velocities perpendicular to the boundary must be the same; if the boundary of the ferrofluid moves outwards from the origin at a certain speed, the external fluid must move away at the same rate.

3.1.1 The moving boundary

Hele-Shaw phenomena have the property that the domain $\mathcal{D}$ is a function of time, as the interaction of fluids producing Saffman-Taylor fingers and other morphological transitions changes the shape of $\mathcal{D}$. This is a property we have not yet accounted for. We note that the boundary is a material boundary; it changes with the fluid. Specifically, the boundary moves in the outward normal direction at the rate of the normal velocity (so that tangential components have no effect). We then have

$$\frac{d}{dt}(\partial\mathcal{D})(\mathbf{x}, t) = \mathbf{v} \cdot \hat{\mathbf{n}}(\mathbf{x}, t)\hat{\mathbf{n}}, \tag{3.1.1}$$

We slightly abuse notation by treating $\partial\mathcal{D}$ as a vector field rather than a set; the context should be clear.

By a similar trick to the proof for the Reynolds transport theorem, along with the assumption that the density is constant, we note that

$$\frac{d}{dt}\int_{\mathcal{D}(t)} d\mathbf{x} = \frac{d}{dt}\int_{\mathcal{D}(0)} J d\mathbf{x} = \int_{\mathcal{D}(0)} \frac{dJ}{dt} d\mathbf{x}.$$

Apply Lemma 2.4.1 to obtain

$$\frac{d}{dt}\int_{\mathcal{D}(t)} d\mathbf{x} = \int_{\mathcal{D}(0)} (J\nabla \cdot \mathbf{u}) d\mathbf{x}.$$

The fluid is incompressible, so

$$\frac{d}{dt}\int_{\mathcal{D}(t)} d\mathbf{x} = 0. \tag{3.1.2}$$

So, the area of the domain is constant by incompressibility. We note this as techniques to analyze the problem (e.g., the mean-field theory of Felix Otto [16] or numerical analysis) do not necessarily include this important feature of the dynamics, so we will need to keep track of it.

3.1.2 The external fluid and boundary conditions

We have not yet said much about the fluid surrounding the ferrofluid in the Hele-Shaw cell. This fluid, often in experiments alcohol, is not affected by the magnetic field and is less viscous than the ferrofluid. However, its behavior is particularly important to the dynamics of the boundary, and we must account for it.

We divide possible boundary conditions of the pressure Poisson equation in two cases. One is quite simple, but not entirely physically accurate; the other is more accurate and has the added benefit of considering surface tension, but at the cost of computational feasibility.

Case 1: The pressure at the boundary is given by the hydrostatic pressure of the outer

interface, say p_0, with the associated magnetic pressure included. This relationship is given by

$$p = p_0 + \mu_0 \int_{\mathbf{0}}^{\mathbf{H}} \mathbf{M} \cdot d\mathbf{H} \tag{3.1.3}$$

Okay, there's some work that needs to be done here developing the magnetic pressure.

This case should be interpreted as a magnetization-dominated case, where fluid properties regarding the evolution of the pressure are essentially treated as parameters and the dynamics of the magnetization exclusively determines the dynamics of the fluid.

Case 2: Let κ be the curvature of the boundary. Then the pressure on the boundary is given by

$$p = -\sigma\kappa + \mu_0 \int_{\mathbf{0}}^{\mathbf{H}} \mathbf{M} \cdot d\mathbf{H} + p_0,$$

where σ is the surface tension of the fluid. This well-known relation is obtained by considering, for instance, a force balance between the surface tension and the pressure on the fluid. In order for the force to balance, the fluid must curve. The coupling of the motion with the geometry of the interface is, in fact, a defining feature of typical Hele-Shaw flow; early investigations (Saffman, Taylor, [25]) of the phenomenon viewed the effects of spherical harmonic perturbations on a circular boundary; the resulting change in the pressure gradient pushes the perturbed boundary into a large finger (called, appropriately, a Saffman-Taylor finger)[1]. In their analysis, they considered a surface tension-free model with an artificially induced perturbation; recent work in considering the effects of surface tension have been somewhat successful in the case where the velocity is entirely described by the gradient of a scalar (Escher, Simonett [5]).

Finally, we demand continuity of the velocity at the boundary, so that

---

[1]An interesting related problem is that of morphological changes of an object due to diffusive or quasistatic heat-determined growth. Here, an object is immersed in a bath such that particles in the bath are attracted either diffusively or conductively; either way, the quasi-staticity implies that the time derivative in the classical heat equation is negligible, so the process is Laplacian. Small perturbations in the boundary then increase the potential field; this is the same principle as the lightning rod. For more details, see "Morphological Stability of a Particle Growing by Diffusion or Heat Flow," W.W. Mullins, R.F. Serkerka, *Journal of Applied Physics*, 1963.

$$-c\hat{\mathbf{n}} \cdot \nabla p_0 = \hat{\mathbf{n}} \cdot \mathbf{v}, \quad \mathbf{x} \in \partial\mathcal{D} \tag{3.1.4}$$

with $\hat{\mathbf{n}}$ a unit normal vector at the boundary. Now, it may seem that $\nabla \times (\mathbf{M} \times \mathbf{H})$ should contain no normal component at the boundary, since it is a torque. However, this is not necessarily the case; the torque is applied to the particles in the ferrofluid, not the ferrofluid itself.

In our analysis, we will investigate both cases to determine in what manner precisely ferrohydrodynamic Hele-Shaw cells with magnetic field deviate from the behavior of typical fluids. The qualitative behavior explained by Zahn et. al [21] regarding the 'twisting' of the Saffman-Taylor fingers is explained by the application of a magnetic torque on the particles suspended in the fluid; a formal numerical study of this effect has, to our best knowledge, never been attempted.

3.2 Formal Model

Here we bring together all of our results for a formal model.

Let $\mathcal{D} = \mathcal{D}(t) \subset \mathbb{R}^2$, $t \in (0, \infty)$ be a bounded domain. We wish to study the following system: inside the domain $\mathcal{D}$ we have

$$\mathbf{v} = \frac{h^2}{12\eta} \left[-\nabla p + \mu_0 \nabla \mathbf{H} \cdot \mathbf{M} + \frac{\mu_0}{2} \nabla \times (\mathbf{M} \times \mathbf{H}) \right] \tag{3.2.1}$$

$$\nabla^2 p = \mu_0 \nabla \cdot (\nabla \mathbf{H} \cdot \mathbf{M}) \qquad\qquad (\mathbf{x}, t) \in \mathcal{D} \times (0, \infty) \tag{3.2.2}$$

$$\frac{d\mathbf{M}}{dt} = \frac{1}{2} (\nabla \times \mathbf{v}) \times \mathbf{M} - \frac{\mathbf{M} - \mathbf{M_0}}{\tau} - \frac{\mu_0}{4\xi} \mathbf{M} \times (\mathbf{M} \times \mathbf{H}). \tag{3.2.3}$$

Boundary conditions for (3.2.2) and the description of the dynamic boundary are given by

$$\frac{d(\partial \mathcal{D})}{dt} = \mathbf{v} \tag{3.2.4}$$

$$p = -\sigma \kappa + p_0 + \int_{\mathbf{0}}^{\mathbf{H}} \mathbf{B} \cdot d\mathbf{H}' \qquad (\mathbf{x}, t) \in \partial \mathcal{D} \times (0, \infty) \tag{3.2.5}$$

$$\hat{\mathbf{n}} \cdot \nabla p = \frac{\eta_1}{\eta_2} \hat{\mathbf{n}} \cdot (\nabla p_0 + \mu_0 \nabla \mathbf{H} \cdot \mathbf{M}) \tag{3.2.6}$$

$$\partial \mathcal{D}(0) = \left\{ (x, y) : x^2 + y^2 = r \right\} \tag{3.2.7}$$

Finally, (3.2.3) needs an initial condition, so we have

$$\mathbf{M} = 0 \qquad (\mathbf{x}, t) \in \mathcal{D} \times \{0\} \tag{3.2.8}$$

Discussion   Arguably the most apparent deviation our approach has compared to most of the existing literature is that we do not assume that the magnetization is collinear with the applied magnetic field. The lag due to the temporal delay in the alignment of the magnetized particles in the fluid may have profound effects on the dynamics of the fluid, and we hope that it is an important expansion on the current theory.

From now, our project will have the following plan of attack:

- Study the magnetization ODE in the absence of velocity effects (the decoupled case)

- Investigate the dynamics of the curvature, using a series of physical assumptions to decouple the curvature from the velocity

- Study the Poisson pressure moving boundary value problem

Chapter 4

Magnetization Dynamics

We study the Langevin magnetization equation in the absence of effects coming from velocity; namely, the following nonlinear system:

$$\frac{d\mathbf{M}}{dt} = \frac{\mathbf{M}_0 - \mathbf{M}}{\tau} + \frac{\mu_0}{4\xi}(\mathbf{M} \times \mathbf{H}) \times \mathbf{M}, \tag{4.0.1}$$

with equilibrium magnetization

$$M_0 = M_s \left[\coth \alpha - \frac{1}{\alpha} \right], \ \ \alpha = \frac{\mu_0 m H}{k_b T} \tag{4.0.2}$$

The first immediate difficulty is $\mathbf{H}$; in the experiment we can fix the magnetic field *outside* of the fluid, but inside the magnetic material things get substantially more complicated. We will initially consider ways to deal with these complicated implicit nonlinear behaviors of the internal applied magnetic field. Afterwards, we will apply this knowledge to discuss the dynamics of the magnetization. Doing so will allow us to formulate expressions of the magnetic force and energy. We mention that the numerical component of this work shall be described in a separate chapter.

4.1 Investigation of H and the demagnetization field

The field we apply is a DC axial field with a rotating uniform transverse field. We have

$$\mathbf{H}_0 = H_3\hat{\mathbf{z}} + H_1 \cos(\omega t)\hat{\mathbf{x}} + H_1 \sin(\omega t)\hat{\mathbf{y}} \tag{4.1.1}$$

However, due to demagnetization effects inside the material, $\mathbf{H}$ is quite different inside

the domain. From classical electromagnetism, the external field magnetizes the fluid, which creates an opposing demagnetization field. This gives

$$\mathbf{H} = \mathbf{H}_0 - \mathbf{H}_D \tag{4.1.2}$$

This field is dependent both on material properties and the shape of the domain. In a very simple case (Rosensweig [22]), a constant weak field is applied to a droplet of ferrofluid. The droplet becomes magnetized and elongates to decrease its magnetic energy; equilibrium is attained by surface tension. Here, we do not have the luxury of a constant weak field, but the physical idea is quite similar.

Quantitatively, standard electromagnetic theory gives the following description for the demagnetizing field $\mathbf{H}_D$, given a volume V with surface S:

$$\mathbf{H}_D(\mathbf{r}) = \oint_S \mathbf{M}(\mathbf{r}') \cdot \widehat{\mathbf{n}}(\mathbf{r}') \frac{\mathbf{r} - \mathbf{r}'}{|\mathbf{r} - \mathbf{r}'|^3} d^2\mathbf{r}' + \int_V \left(\nabla' \cdot \mathbf{M}(\mathbf{r}') \right)(\mathbf{r}') \frac{\mathbf{r} - \mathbf{r}'}{|\mathbf{r} - \mathbf{r}'|^3} d^3\mathbf{r}', \tag{4.1.3}$$

where we adopt the standard convention that ∇' indicates taking the derivatives with respect to the primed coordinates. The physical interpretation for (4.1.3) is that the surface integral represents demagnetization due to normal poles on the surface of the fluid while the volume integral considers volume charges which have effect when the magnetization is not divergence-free.

Many authors successfully used some sort of *ansatz* for the internal field, such as linear radial dependence (Oliveira et. al. [15]). However, we currently have no meaningful preliminary assumption based on qualitative grounds, particularly as we are not considering a constant field. Initially we will follow their approach, considering the new case of a time-dependent field. Afterwards, we will attempt to derive a reasonable closed-form description of $\mathbf{H}$. However, we will not attempt to solve the full integral equation, and instead use experimental data and qualitative behavior to find ways to directly express the internal magnetic field.

As a side note, we mention that we are not fully interested in modelling the internal magnetic field as accurately as possible, which is probably excessively complicated. We will use our approximations to explore the fluid dynamics, and not worry too much about the mag-

netization dynamics. For completeness, we will briefly describe the types of considerations used in rigorously describing the demagnetization field.

4.2 Easiest approximation

Following (Oliveira et. al. [15]), we initially we consider the action of a radial magnetic field:

$$\mathbf{H} = H_3\hat{\mathbf{z}} + H_1 r\cos(\omega t - \theta)\hat{\mathbf{r}} + H_1 r\sin(\omega t - \theta)\hat{\theta} \tag{4.2.1}$$

First, we note that this formulation is actually not quite the magnetization that we wish to model. To wit, we should not expect the behavior that results from this expression to match the behavior observed in experiment. However, this expression is experimentally realizable to good approximation. Further, its simplicity is particularly appealing, as we can perform some relatively sophisticated analysis to test out basic physical hypotheses regarding the importance of the terms which are nonlinear in magnetization.

Initially we consider briefly the collinear case to point out its shortcomings (in the context of what we wish to demonstrate), then proceed to a more physically realistic scenario via the Langevin equation.

We have

$$\mathbf{M}(r,t) = \chi H_0 r\hat{\mathbf{r}} + \chi H_1 r\omega t\hat{\theta} + \chi H_3\hat{\mathbf{z}}. \tag{4.2.2}$$

The pressure Poisson equation (3.0.9) then becomes

$$\nabla^2 p = \chi H_0^2, \tag{4.2.3}$$

and the velocity is governed by

$$\mathbf{v} = \frac{h^2}{12\eta}\left[-\nabla p + \chi H_0^2 r\hat{\mathbf{r}} + \chi H_0 H_1 r\omega t\hat{\theta}\right] \tag{4.2.4}$$

In particular, we see immediately that relaxing the assumption of collinearity is necessary for the appearance of "curling" fingers; the only nonradial term here oscillates with the applied magnetic field, and for even moderate frequencies, this effect would be undetectable *(by a dimensional analysis argument)*[1]. Further, no time-dependent terms appear in the

---

[1] One could object that this would not be true if the length of the fingers were quite long, so that there

pressure Poisson equation, implying that without collinearity we really have no new phenomena beyond static Hele-Shaw ferrofluid dynamics. Naturally, this is entirely consistent with experiment; the cause of the "curling" is hypothesized to be magnetic torque on the immersed particles creating angular momentum within the fluid. Finding the collinear case inadequate, we move on to the more realistic case governed by the Langevin equation.

4.2.1 Approximate analysis

We initially assume a weak collinearity, so that the Langevin equation (4.0.1) loses the vorticity term and reads as

$$\frac{d\mathbf{M}}{dt} = \frac{\mathbf{M}_0 - \mathbf{M}}{\tau},\tag{4.2.5}$$

which we shall call the *irrotational Langevin equation*. We are still using

$$M_0 = M_s\left[\coth\alpha - \frac{1}{\alpha}\right], \quad \alpha = \frac{\mu_0 m H}{k_b T}$$

as before. We remark that $\mathbf{M}_0$ is collinear with $\mathbf{H}$, so we have $\mathbf{M}_0 = \dfrac{M_0}{H}\mathbf{H}$, giving

$$\mathbf{M}_0 = \frac{M_0}{\sqrt{H_1^2 r^2 + H_3^2}}\left(H_3\hat{\mathbf{z}} + H_1 r\cos(\omega t - \theta)\hat{\mathbf{r}} + H_1 r\sin(\omega t - \theta)\hat{\theta}\right).\tag{4.2.6}$$

Note that M_0 is constant in time, and is only rotating with $\mathbf{H}$. The resulting linear equation is easily solved, and we see that we obtain a decaying exponential in the three components, along with a few extra terms. The point of this is that the governing equation for magnetization roughly describes decaying exponential relaxation towards equilibrium, so this is the sort of broad behavior we would expect. Our interest is the effect of the torque term on this relaxation.

4.3 A better expression for $\mathbf{H}_d(\mathbf{x}, t)$

Zahn et. al. [17] provide a simple approximate formula for the demagnetization field,

$$\mathbf{H}_d = D\mathbf{M}_0,\tag{4.3.1}$$

---

was notable displacement in relevant timescales. This is true, but it would also be the case that Darcy's law would fail to hold, as the second partials would no longer be negligible.

with

$$D = \frac{1}{\sqrt{\left(\frac{2r}{h}\right)^2 + 1}} - 1 \tag{4.3.2}$$

and $\mathbf{M}_0$ obtained from (4.0.2) computed using $\mathbf{H}_E$ as in (4.1.1). This is actually a more relevant expression than the one we have obtained from Oliveira et. al., and possibly a more accurate approximation of the demagnetization effects. This formula is essentially based on a local dipole approximation, and is relatively accurate for weak fields. More to the point, we are considering the same type of field that Zahn did in his paper, which agreed with his experimental evidence.

We compute the demagnetization field:

$$\mathbf{H}_d = D\frac{M_0}{\sqrt{H_0^2 + H_1^2}} \left(H_0\hat{\mathbf{z}} + H_1 \cos(\omega t - \theta)\hat{\mathbf{r}} + H_1 \sin(\omega t - \theta)\hat{\theta} \right), \tag{4.3.3}$$

and use this expression, along with an easy solution of the irrotational Langevin equation (4.2.5), to obtain expressions for the magnetic force and torque terms.

Chapter 5

Numerical analysis of magnetization

Looking back at the full Langevin equation (4.0.1), we seek to obtain a numerical solution for use in future computations. This is a desirable result as, in order capture a fuller picture of the phenomena of interest, a large number of approximate results culminating in an approximate complete solution is preferred to an in depth investigation of magnetization alone with little time left for other contributing factors.

This numerical result is obtained through simple finite difference in time, coupled with a discretization of the domain we wish to investigate. Dealing with the time portion of the result, we begin by rewriting the Langevin equation as

$$d\mathbf{M} = \left[\frac{\mathbf{M}_0 - \mathbf{M}}{\tau} + \frac{\mu_0}{4\xi} (\mathbf{M} \times \mathbf{H}) \times \mathbf{M} \right] dt. \qquad (5.0.1)$$

We are thus able to treat the differential equation via the simple repeated linear extrapolation

$$\mathbf{M}^{(n+1)} = \mathbf{M}^{(n)} + dt \cdot \left[\frac{\mathbf{M}_0^{(n)} - \mathbf{M}^{(n)}}{\tau} + \frac{\mu_0}{4\xi} (\mathbf{M}^{(n)} \times \mathbf{H}^{(n)}) \times \mathbf{M}^{(n)} \right], \qquad (5.0.2)$$

where the superscript indicates the timestep in consideration. It should be noted that the time evolutions of $\mathbf{M}_0$ and $\mathbf{H}$ are already specified by their definitions, and do not require iterative definitions.

From here, we discretize the domain in which we will analyze the magnetization. As no spatial derivatives are present, each chosen point evolves independent of the rest. Thus, our chosen level of discretization is not limited by considerations of numerical accuracy, but sim-

ply by time and storage constraints during computation and the desired degree of resolution in the resulting data. Although initially a 5cm × 5cm square was used, the computation time was rather lengthy. Noting that the equations have radial symmetry, however, in the final program, only a single ray from the origin of total length 5cm was used. The behavior in the total domain of interest is then found by revolving the resultant curve around the center point. For the simulation discussed, this 5cm ray is discretized into $512 + 1$ points, the $+1$ referring to the origin.

A word on the various constants required by the equation is now in order[1]. From Rosensweig [22] and He [8] we have values of $\tau = 4.10 \times 10^{-6}$ s and $\xi = 0.002$ kg/(m s). Of course, $\mu_0 = 4\pi \times 10^{-7}$ m kg/C^2 is well known from electromagnetism, while $\omega = 25/2\pi$ Hz, $H_1 = 0.005$ T/μ_0 and $H_3 = 0.025$ T/μ_0 are determined by the experimental situation we consider[2]. This leaves only the consideration of $\mathbf{M}_0$. Referring to Eq. (4.0.2) we need values for M_s and α. We utilize $M_s = M_d\phi$, where M_d is the magnetization of each nanoparticle and ϕ is the volume fraction of nanoparticles. The quantity M_d is further defined via $m = M_d \cdot V_p$, where m is again the magnetic moment and V_p is the volume of the nanoparticle, a relation which harkens back to the basic equations of ferromagnetism from Chapter 2. From Zahn [21], a representative value is $\mu_0 M_d\phi = 0.0244$ T, thus giving us $M_s = 0.0244$ T/μ_0. Lastly, for our value of α we use the magnetization of magnetite $m = 4.46 \times 10^5$ A/m $\cdot$ 5.25×10^{-25} m^3 = 2.34×10^{-19} A m^2, where the first number in the multiplication is the domain magnetization of magnetite while the second is the nanoparticle volume, taken to be the volume of a sphere with diameter on the order of 10nm. The value of H varies with location but remains fully known, while we use room temperature $(20°C)$ to get $k \cdot T = 4.045 \times 10^{-21}$ J, where k_b is the Boltzmann constant. Since $\mu_0 \cdot H \sim 10^{-2}$, we end up with $\alpha \sim 1$, and will need to compute its value as dependent on the varying of H with the radius[3]. These values taken together, taking care to keep $\mathbf{M}_0$ collinear with $\mathbf{H}$ once we have the magnitude, allow us to completely solve the numerical problem. The code which does this is written using FORTRAN77 and looks at the cartesian coordinates of the magnetization rather than the polar coordinates used in the analytic analysis. It is attached for reference in section A.1.

---

[1]In our usage, all constants and quantities of interest are in MKS units.

[2]Note that the units here are A/m

[3]Note that for orders of magnitude of α greater than ~ 100, the entire portion of $\mathbf{M}_0$ involving α is quite accurately approximated by setting it to 1, greatly simplifying the calculation by allowing changing H to be ignored

5.1 Results

5.1.1 First Demagnetization Model (Oliveira)

Initial runs of the program were used to determine the timestep necessary for numerical stability. Beginning at a timestep of 10^{-2} and decreasing by one order of magnitude per run showed that steps as low as 10^{-5} still caused the results to diverge, but a timestep of 10^{-6} finally led to stable results. These were then verified to be numerically stable by running with a timestep of 10^{-7} and seeing no change in the output. Although the timestep 10^{-6} was thus the largest stable timestep, having already invested the runtime to calculate the 10^{-7} results, these are the numbers used for the subsequent analysis.

Due to the large volume of the data collected, a program was then written in MATLAB which imported the data and automatically processed it into a meaningful format. This code is shown in section A.2, and a number of plots demonstrating the behavior of the magnetization were produced from it.

To begin with, we analyze the behavior of the z-component of the magnetization in both space and time. Plotting the spatial profile at any given snapshot in time, we can see that beginning immediately at the first non-zero timestep, the profile in space only varies very slightly, and variation compared to its absolute magnitude is very small. For this reason, particularly given the crudeness of the magnetization model, we can safely consider it spatially a constant. This feature is demonstrated by Figure 5.1. We can then plot one spatial grid of the z-component in time, shown in Figure 5.2, and see that it is completely constant in that regard, too. For this reason, we say that the z-component is constant at 8270.2 A/m, regardless of spatial location, and that it reaches this value in a timescale far below what we concern ourselves with.

The x- and y-components are slightly more complicated. In Figure 5.3, we plot both components, as well as the r-component ($\sqrt{x^2 + y^2}$), in space for a single time snapshot. The individual components, along with the r-component, are seen to have a linear profile in r, with the peak value in r of 82.5539 A/m at 5 cm. Figure 5.4 shows that the total in-plane component retains this constant profile in time, but Figure 5.5 shows how the decomposition into the coordinate axes oscillates with time. This oscillation turns out to be at precisely the same frequency as the rotation of the applied magnetic field. This leads to the conclusion

that the first magnetization model results in complete collinearity with the magnetic field and a linear profile in space, and can be expressed by

$$\mathbf{M} = 8270.2 \text{ A/m } \hat{\mathbf{z}} + 1651.1 \text{ A/m}^2 \ r \left(\cos\left(\omega t \right) \hat{\mathbf{x}} + \sin\left(\omega t \right) \hat{\mathbf{y}} \right). \qquad (5.1.1)$$
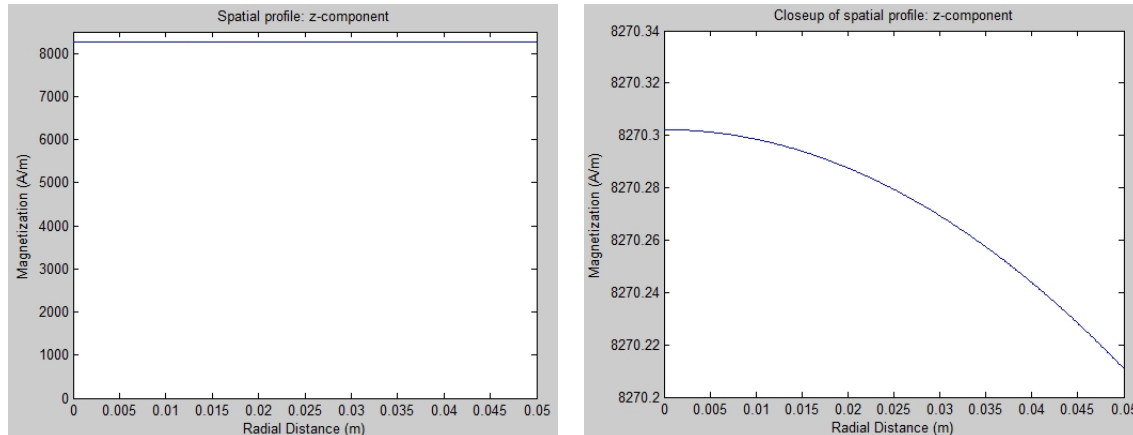

Figure 5.1: The figure on the left shows the behavior of the z-component of the magnetization at $t = 0.5$ s for the first demagnetization model, while the figure on the right is a closeup, showing the small scale variation. On any scales of interest to us, this variation is safely ignored by being much smaller than the error inherent in the crudeness of the model.

5.1.2   Second Demagnetization Model (Zahn)

For the second model, concerns of numerical stability and the simulation output were handled identically to the first, even up to using the same timestep. We therefore immediately present the same sequence of graphs as for the first (Figures 5.6 through 5.10). Although the details of the z-component in space are slightly different, it still holds that we can treat it as constant for our purposes, in this case slightly lower in value than for the first model. The differences really make themselves apparent in the in-plane component of the magnetization. Although the time behavior is still essentially identical, namely a clear indication of collinearity along with an x/y tradeoff that leaves the total in-plane component constant, the spatial profile is clearly different. The peak is now almost twice as high, and in addition to no longer being perfectly linear, the magnetization at the origin is non-zero. To arrive at a nice expression for this new magnetization, we note that most of the spatial profile *is* linear, and simply extrapolate that line to the origin. This gives the result presented in Equation (5.1.2), and
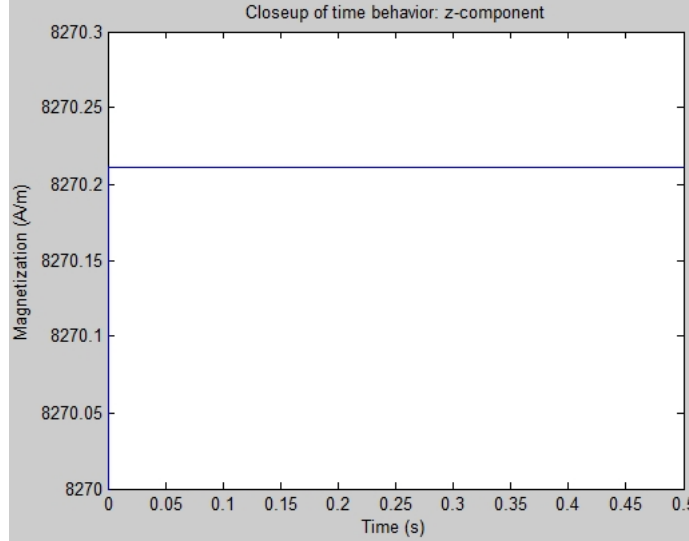
Figure 5.2: This graph shows the constancy of the z-component of the magnetization in time for the first model. The point plotted is the location at $r = 0.05$ m.

the accuracy of this linear approach is seen to be quite good, particularly past $r = 0.005$ m, in Figure 5.11.

$$\mathbf{M} = 8267.2 \text{ A/m } \hat{\mathbf{z}} + \left(1518.9 \text{ A/m}^2 \, r + 129.0 \text{ A/m}\right) \left(\cos\left(\omega t\right) \hat{\mathbf{x}} + \sin\left(\omega t\right) \hat{\mathbf{y}}\right). \qquad (5.1.2)$$

5.2   Conclusion

The major failing that we perceive in the results of either model is the predicted collinearity. As previously mentioned, the observed spiral structures that form in ferrofluids is the direct result of the torque terms of the form $\mathbf{H} \times \mathbf{M}$. If these two are in fact collinear, torque should fail to manifest itself. We also note that in the development of those models, no consideration is made for the location of the edge of the ferrofluid. For this reason, we feel that these models are only particular effective in the interior of the ferrofluid, and thus make the conclusion that torque and curling in ferrofluids is the result of edge effects not considered by these models. We further conclude that the second model is more realistic than the first, as we expect non-zero magnetization throughout the ferrofluid and not some special cancelation at the center of the domain.
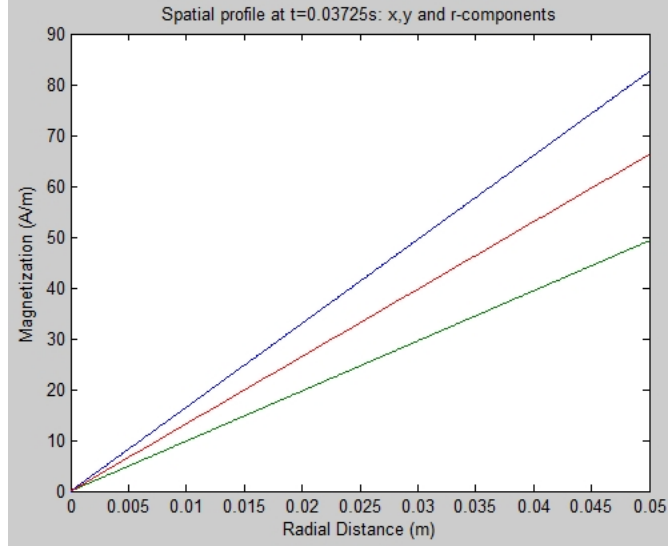
Figure 5.3: This plot shows the x- and y-components of the magnetization in space, along with the total $r = \sqrt{x^2 + y^2}$ in-plane component, for the first model. The blue line is r, the red is y and the green is x. The time considered is $t = 0.03725$ s.

These results are to be somewhat expected. In the first model, the original authors specifically constructed their demagnetization to obtain exact solutions that weren't based on *completely* physically baseless assumptions. In the case of the second model, Zahn was looking at an energy minimization model to predict morphological changes, and was in a near equilibrium case where the magnetization was no longer changing very much. These points further bolster our claim that the models are only somewhat valid in general bulk regions. One approach we'd hoped to take to correct for this was to look at the approach of Richardi et. al. [18], but due to time constraints, we were unable to do so.
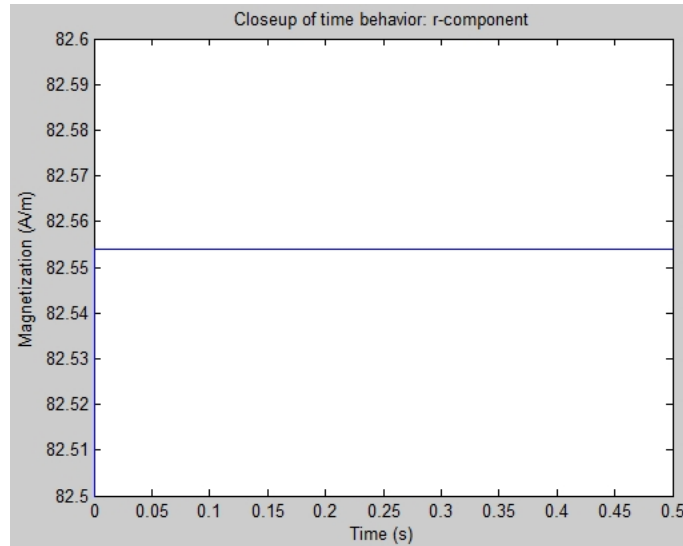
Figure 5.4: This graph shows the constancy of the r-component of the magnetization in time for the first model. The data has been zoomed to demonstrate this even on a small scale, and to better show the exact value at a radial distance of $r = 0.05$ m.

Figure 5.5: This plot shows the sinusoidal tradeoff between the x- and y-components of the magnetization in time for the first model. The frequency of oscillation in the graph is exactly that of the frequency with which the applied magnetic field rotates, and the peak values are exactly that shown in Figure 5.4.
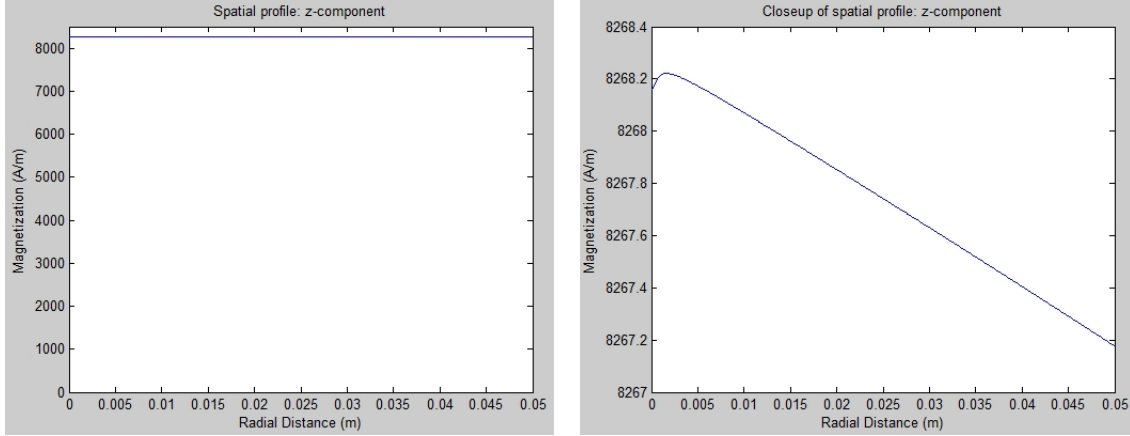
Figure 5.6: The figure on the left shows the behavior of the z-component of the magnetization at $t = 0.5$ s for the second demagnetization model, while the figure on the right is a closeup, showing the small scale variation. On any scales of interest to us, this variation is safely ignored by being much smaller than the error inherent in the model.
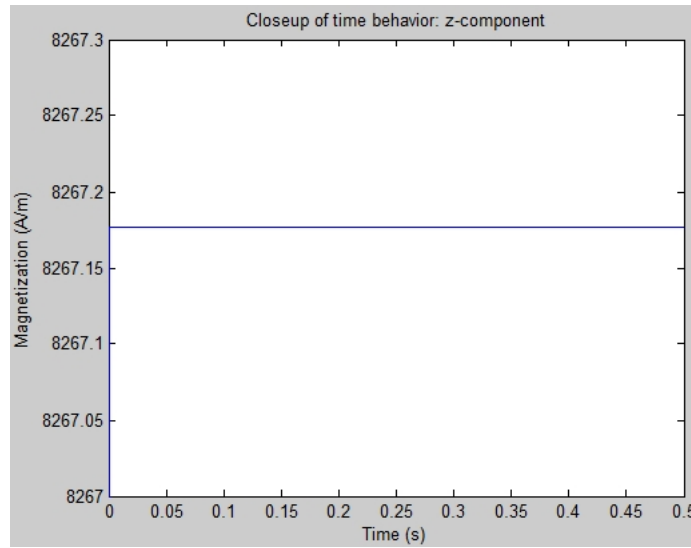
Figure 5.7: This graph shows the constancy of the z-component of the magnetization in time for the second model. The point plotted is the location at $r = 0.05$ m.
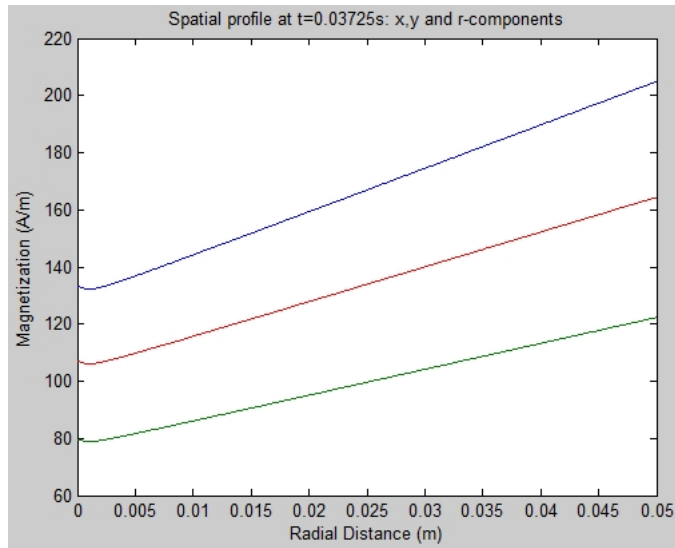
Figure 5.8: This plot shows the x- and y-components of the magnetization in space, along with the total $r = \sqrt{x^2 + y^2}$ in-plane component, for the second model. The blue line is r, the red is y and the green is x. The time considered is $t = 0.03725$ s. Note that the primary variation from the first model is the non-zero intercepts.
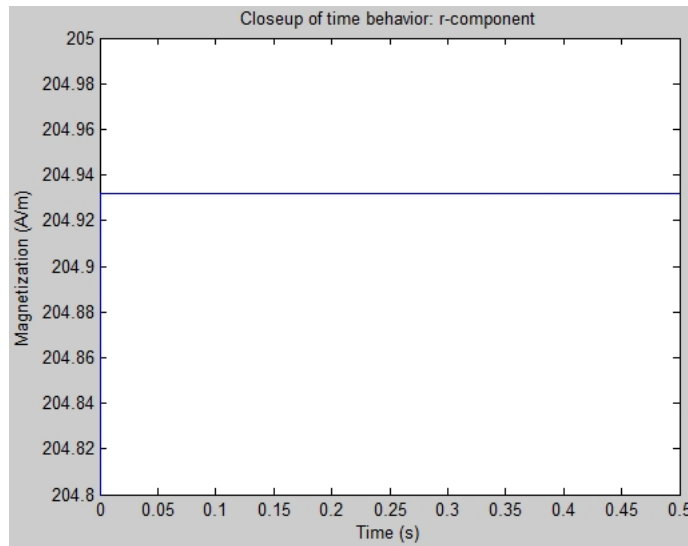
Figure 5.9: This graph shows the constancy of the r-component of the magnetization in time for the second model. The data has been zoomed to demonstrate this even on a small scale, and to better show the exact value at a radial distance of $r = 0.05$ m.
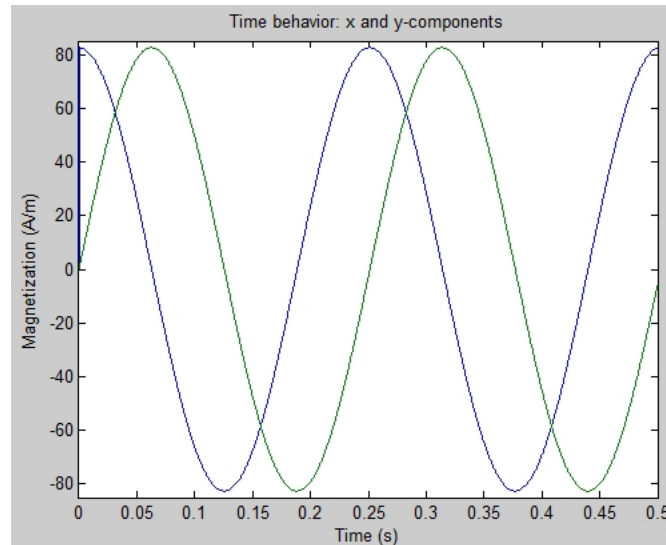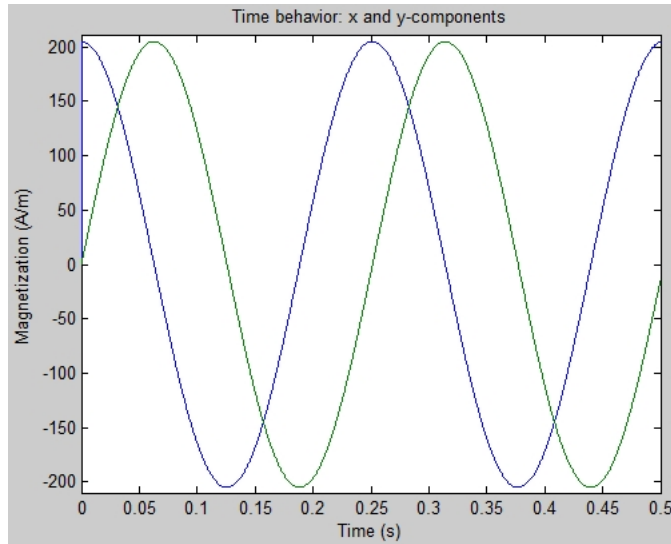
Figure 5.10: This plot shows the sinusoidal tradeoff between the x- and y-components of the magnetization in time for the second model. The frequency of oscillation in the graph is exactly that of the frequency with which the applied magnetic field rotates, and the peak values are exactly that shown in Figure 5.9.
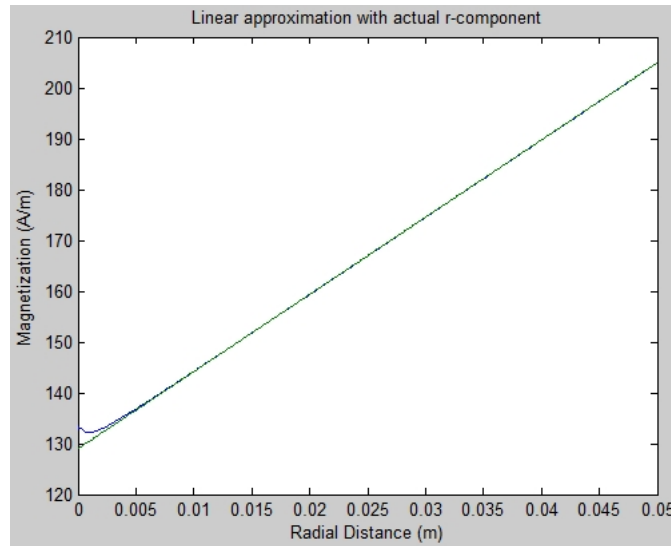

Figure 5.11: This plot shows the effectiveness of the linear approximation to the actual spatial behavior of the r-component of the magnetization in the second model. It is particularly accurate after $r = 0.005$ m.

Chapter 6

Interface curvature and vortex sheets

In order to study the dynamics of the curvature of the domain, we will first study the vortex sheet strength at the boundary. The vortex sheet strength is defined on the boundary as

$$\Gamma(\mathbf{x}, t) = (\mathbf{v}_1(\mathbf{x}, t) - \mathbf{v}_2(\mathbf{x}, t)) \cdot \hat{\mathbf{s}} \tag{6.0.1}$$

where $\mathbf{v}_1$ is the velocity of the ferrofluid, $\mathbf{v}_2$ is the velocity of the surrounding fluid, and $\hat{\mathbf{s}}$ is the unit tangent vector of the boundary at $\mathbf{x}$. We have taken the continuous extension of $\mathbf{v}_1$ and $\mathbf{v}_2$ to the boundary. Conditions on the vortex sheet strength are analogous to the continuity condition (3.1.4) for normal velocities, and if we know its value we can use its explicit expression to learn about the dynamics of the fluid. We can compute this directly, but first introduce some new notation. Let

$$\mathcal{A} = \frac{\eta_1 - \eta_2}{\eta_1 + \eta_2} \tag{6.0.2}$$

be defined as the viscosity contrast. Then

$$\mathbf{v}_1 - \mathbf{v}_2 = 2\frac{\eta_1 \mathbf{v}_1 - \eta_2 \mathbf{v}_2}{\eta_1 + \eta_2} - \mathcal{A}(\mathbf{v}_1 + \mathbf{v}_2)$$

Fortunately, the first term of the right-hand side of this equation effectively eliminates the mathematical dependence of viscosity on the velocity in Darcy's law. We also define $\mathbf{V}$ to be the arithmetic mean of the limiting value of the velocities taken at either side of the interface. Now, applying the continuity of velocity boundary condition (3.1.2) and taking the scalar product with a unit tangent vector gives

$$\Gamma = \frac{2}{\eta_1 + \eta_2} \nabla \left(\sigma\kappa - \mu_0 \int_{\mathbf{0}}^{\mathbf{H}} \mathbf{M} \cdot d\mathbf{H} \right) \cdot \hat{\mathbf{s}} + \frac{\mu_0}{\eta_1 + \eta_2} \nabla \times (\mathbf{M} \times \mathbf{H}) \cdot \hat{\mathbf{s}} + 2\mathcal{A}\mathbf{V} \cdot \hat{\mathbf{s}}. \quad (6.0.3)$$

The importance of this equation is that the surface tension boundary term $\sigma\kappa$ allows us to formulate a differential equation describing the pressure. A similar methodology was used in [Miranda, Oliveira] in the case of irrotational flow; we will expand this to include force terms which cannot be expressed as the gradient of a scalar.

6.1 Brief overview of vortex sheets in irrotational Hele-Shaw flow

We present some of the basics of the theory of vortex sheets in two-dimensional irrotational incompressible flow. Much of the basic framework can be found in Saffman and Baker [24], but we rederive some of the results given without proof.[1]

Let $(u, v) = \nabla\phi$ be an irrotational incompressible velocity field in two dimensions, and suppose ϕ is discontinuous across some interface Υ, parameterizable as a simple closed curve, but that its directional derivative normal to the interface is continuous. This means that the velocity potentially has a tangential discontinuity across Υ, which we shall call a vortex sheet. We work in the complex numbers, mapping (a, b) in $\mathbb{R}^2$ to $a + bi$ in $\mathbb{C}$, motivated by the fact that ϕ is analytic under this mapping. We take the continuous extension of (u, v) to Υ again in defining $\Gamma(z, t)$ as the difference of the continuous extensions of the velocities at either side of Υ.

Parameterize Υ by s, so that $X(s, t) + iY(s, t) = Z(s, t)$. We have by Cauchy's integral formula that

$$u(z) - iv(z) = \frac{1}{2\pi i} \int_\Upsilon \frac{\Gamma(s', t)}{z(s, t) - Z(s', t)} ds' \quad (6.1.1)$$

describes the velocity due to the interface interactions at a point z away from the interface. On the interface, we define similarly

---

[1]Saffman also wrote a textbook <u>Vortex Dynamics</u>, 1995, but it was unavailable for much of the duration of this project. In the irrotational case, results are easy enough to derive anyway.
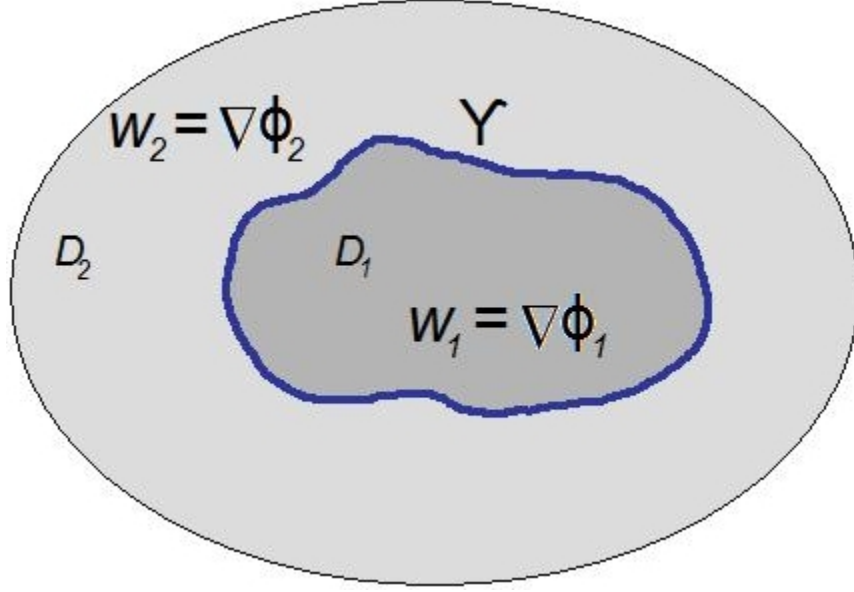
Figure 6.1: An illustration of the domain.

$$\tilde{U}(z) - i\tilde{V}(z) = \frac{1}{2\pi i} \fint_{\Upsilon} \frac{\Gamma(s',t)}{z(s,t) - Z(s',t)} ds' \qquad (6.1.2)$$

as the average induced velocity of the sheet, where $\fint$ indicates the principal value integral. This is equivalent to the limit of the arithmetic mean of (6.1.1) taken at either side of Υ; define $V(s,t)$ to be this value and write Υ parameterized in polar coordinates as $R(s,t)e^{i\theta(s,t)}$. Define Υ_{ε}^+ to be the curve parameterized by $(R(s,t) + \varepsilon)e^{i\theta(s,t)} \equiv Z_{\varepsilon}^+(s,t)$ and Υ_{ε}^- as parameterized by $(R(s,t) - \varepsilon)e^{i\theta(s,t)} \equiv Z_{\varepsilon}^-(s,t)$. Then

$$V(s,t) = \lim_{\varepsilon \to 0} \frac{1}{2} \left(\frac{1}{2\pi i} \int_{\Upsilon_{\varepsilon}^+} \frac{\Gamma(s',t)}{z(s,t) - Z_{\varepsilon}^+(s',t)} ds' + \frac{1}{2\pi i} \int_{\Upsilon_{\varepsilon}^-} \frac{\Gamma(s',t)}{z(s,t) - Z_{\varepsilon}^-(s',t)} ds' \right), \quad (6.1.3)$$

which is precisely the definition of the principal value integral. Translating these results back to $\mathbb{R}^2$ and noting that only the effects of the jump in tangential velocity correlate to solenoidal velocity terms gives the following result of Birkhoff:

Theorem 6.1.1. $\mathbf{V}(s,t)$, *the average of the limiting value of the solenoidal velocity on either side of $\partial \mathcal{D}$, parameterized by s, is given by*

$$\mathbf{V}(s,t) = \frac{1}{2\pi} \fint_{\partial \mathcal{D}} \frac{\hat{\mathbf{z}} \times [\mathbf{r}(s,t) - \mathbf{r}(s',t)]}{|\mathbf{r}(s,t) - \mathbf{r}(s',t)|^2} \Gamma(s',t) ds' \qquad (6.1.4)$$

Unfortunately we do not have the irrotational approximation, but we note these results, as they will be useful later.

6.2   No-slip approximation

One immediate way for the vortex-sheet consideration to be useful is to assume that the fluids do not slip past each other at the boundary, so that $\Gamma(\mathbf{x}, t) = 0$ for all $\mathbf{x}$ and t. In a recent paper, [15] used a similar analysis in the case of irrotational ferrofluid flow, using Birkhoff's result to obtain a closed-form expression for the curvature of the domain. By (3.1.4), this is equivalent to simply requiring that the velocities at either side of the boundary are the same. We use the simpler expressions of $\mathbf{M}$ and $\mathbf{H}$ derived in Chapter 3, , giving a differential equation for κ:

$$0 = \frac{2}{\eta_1 + \eta_2} \nabla \left(\sigma \kappa - \mu_0 \int_{\mathbf{0}}^{\mathbf{H}} \mathbf{M} \cdot d\mathbf{H} \right) \cdot \hat{\mathbf{s}} + \frac{\mu_0}{\eta_1 + \eta_2} \nabla \times (\mathbf{M} \times \mathbf{H}) \cdot \hat{\mathbf{s}} + 2\mathcal{A}\mathbf{V} \cdot \hat{\mathbf{s}}. \qquad (6.2.1)$$

In order for this to be of use, we would like to know $\mathbf{V}(\mathbf{x}, t)$. Without loss, we take $\mathbf{V}(\mathbf{x}, t)$ to be the limiting value of the solenoidal velocities, as the decomposition of the velocity into a normal and tangential component corresponds precisely to the Helmholtz decomposition, by the definition of our interface. Hence, for the rest of this chapter, we shall take the following conventions and notations:

- We will work in the domain $\Omega = \Omega_1 \dot{\cup} \Omega_2 \dot{\cup} \mathcal{C}$, with Ω_1 indicating the space occupied by ferrofluid, Ω_2 the space occupied by the external fluid, and $\mathcal{C} := \overline{\Omega_1} \cap \overline{\Omega_2}$ the vortex sheet. Ω and Ω_1 are simply connected, and $\mathcal{C}$ is a simple closed curve that disconnects Ω in the obvious way.

- Ω_1, Ω_2, and $\mathcal{C}$ are dependent on a parameter t, the time.

- $\mathcal{C}(t)$ can be parameterized as a curve possessing an analytic diffeomorphism to the unit circle for all t. That is, given the earlier map to $\mathbb{C}$, there exists a conformal map from $\mathcal{C}(t)$ to the unit circle.[2]

- $\mathbf{v}_1 = \nabla \phi_1 + \nabla \times \mathbf{A}_1$ and $\mathbf{v}_2 = \nabla \phi_2 + \nabla \times \mathbf{A}_2$. $\mathbf{A}_1$ is a given quantity.

---

[2]By the Riemann mapping theorem in $\mathbb{C}$, this is probably more than we need, but we decided to play it safe. In further analysis, we actually consider C^2-diffeomorphisms, as there is a proof found in Escher and Simonett that C^2 diffeomorphisms preserve analyticity of the boundary in Hele-Shaw cell in finite time.

- We consider $\mathbf{v}_i \in \mathbb{R}^2$, so that $\mathbf{A}_i = (0, 0, A_i)$, with $A_i = A_i(x, y)$. We will assume $\phi_i \in C^2(\Omega_i)$ and $\mathbf{A}_i \in C^2(\Omega_i)$. We further assume $\mathbf{v}_i \in H^1(\Omega_i)$.

- $\Gamma(\mathbf{x}, t) := \lim\limits_{\varepsilon \to 0} (\mathbf{v}_1(\mathbf{x} - \varepsilon\hat{\mathbf{n}}, t) - \mathbf{v}_2(\mathbf{x} + \varepsilon\hat{\mathbf{n}}, t)) \cdot \hat{\mathbf{s}}$ with $\mathbf{x}$ a point on the vortex sheet and $\hat{\mathbf{s}}$ a unit tangent vector on $\mathcal{C}$ at $\mathbf{x}$.

- $\mathbf{V}(\mathbf{x}, t) := \lim\limits_{\varepsilon \to 0} \dfrac{1}{2} (\mathbf{v}_1^s(\mathbf{x} - \varepsilon\hat{\mathbf{n}}, t) + \mathbf{v}_2^s(\mathbf{x} + \varepsilon\hat{\mathbf{n}}, t))$, where $\mathbf{x}$ is a point on a vortex sheet and $\mathbf{v}_i^s$ is the solenoidal component of $\mathbf{v}_i$.

- $\mathbf{v}_1 \cdot \hat{\mathbf{n}} = \mathbf{v}_2 \cdot \hat{\mathbf{n}}$ on $\mathcal{C}$.

We can determine $\mathbf{A}_i$ with fairly standard techniques from vector analysis; take the curl of $\mathbf{A}_i$ and recall that $\omega_i := \nabla \times \mathbf{v}_i$, which gives

$$\omega_i = \nabla \times (\nabla \times \mathbf{A}_i) = \nabla(\nabla \cdot \mathbf{A}_i) - \nabla^2 \mathbf{A}_i.$$

By choosing an appropriate gauge (as in standard electromagnetic theory) we may choose $\mathbf{A}_i$ to be divergence-free by arbitrarily adding the gradient of a scalar (which is necessarily curl-free), so $\mathbf{A}_i$ can be expressed as a solution to a vector Poisson equation;

$$\nabla^2 \mathbf{A}_i = -\omega_i. \tag{6.2.2}$$

In the irrotational case we see from (6.1.4) that $\mathbf{V}(\mathbf{x}, t)$ is zero when the vortex sheet strength is zero. To explain this physically, albeit somewhat loosely, the discontinuity of the tangential velocities across the vortex sheet gives rise to a solenoidal component of the velocity at either side of the interface. Removing this discontinuity removes the presence of solenoidal velocities. Here, we have that the applied force itself gives a solenoidal velocity disregarding interface effects.

Lemma 6.2.1. *Suppose we have $\Gamma = 0$ everywhere along $\mathcal{C}$. Then ω, defined by*

$$\omega(\mathbf{x}, t) = \begin{cases} \omega_1(\mathbf{x}, t) & \mathbf{x} \in \Omega_1 \\ \omega_2(\mathbf{x}, t) & \mathbf{x} \in \overline{\Omega}_2 \end{cases} \tag{6.2.3}$$

is continuous.

Proof. We first compute Γ and $(\mathbf{v}_1 - \mathbf{v}_2) \cdot \hat{\mathbf{n}}$, which are both zero by hypothesis. Using

$\nabla \times \mathbf{A}_i = \partial_y A_i \hat{\mathbf{x}} - \partial_x A_i \hat{\mathbf{y}}$ we arrive at

$$\Gamma = \partial_s(\phi_1 - \phi_2) + \partial_n(A_1 - A_2) = 0 \tag{6.2.4}$$

$$(\mathbf{v}_1 - \mathbf{v}_2) \cdot \hat{\mathbf{n}} = \partial_n(\phi_1 - \phi_2) - \partial_s(A_1 - A_2) = 0 \tag{6.2.5}$$

Taking the directional derivative ∂_n on both sides of (6.2.4) and the directional derivative ∂_s on both sides of (6.2.5), then taking the difference between the two, gives

$$\nabla_{\mathcal{C}}^2 A_1 = \nabla_{\mathcal{C}}^2 A_2 \tag{6.2.6}$$

where $\nabla_{\mathcal{C}}$ indicates taking the derivative with respect to the normal and tangential coordinates of $\mathcal{C}$. Now, as the domain was assumed to be simply connected and its boundary analytic, we have that $\nabla_{\mathcal{C}}^2 A_1 = \nabla_{\mathcal{C}}^2 A_2$ if and only if $\nabla^2 A_1 = \nabla^2 A_2$ in their continuous extension to the boundary, since $\mathcal{C}$ can be expressed as a conformal map of, say, the unit circle. So we have by (6.2.2) that

$$\lim_{\varepsilon \to 0} \omega_1(\mathbf{x} - \varepsilon \hat{\mathbf{n}}, t) = \lim_{\varepsilon \to 0} \omega_2(\mathbf{x} + \varepsilon \hat{\mathbf{n}}, t) \text{ for all } \mathbf{x} \in \Gamma. \tag{6.2.7}$$

Hence ω as defined above is continuous.

□

This establishes that $\nabla \times \mathbf{A}_1$ and $\nabla \times \mathbf{A}_2$ differ at $\mathcal{C}$ by a curl-free function, so that without loss we have

$$\nabla \times \mathbf{A}_1(\mathbf{x}, t) = \nabla \times \mathbf{A}_2(\mathbf{x}, t) + \nabla \psi(\mathbf{x}, t) \text{ on } \mathcal{C}. \tag{6.2.8}$$

Clearly $\nabla^2 \psi = 0$ on $\mathcal{C}$. Without loss we take $\nabla^2 \psi = 0$ in $\Omega_2 \cup \Omega_1$, consistent with the fluid being incompressible. We then write the solenoidal velocity $\mathbf{v}_i^s$ as

$$\mathbf{v}_1^s = \nabla \times \mathbf{A}_1, \quad \mathbf{v}_2^s = \nabla \psi + \nabla \times \mathbf{A}_2 \tag{6.2.9}$$

However, we may apply Birkhoff's theorem (6.1.4) to *this* expression without having to worry about our gauge choice; this gives $\nabla \psi = 0$, so that

$$\mathbf{V}(\mathbf{x}, t) = \nabla \times \mathbf{A}_1(\mathbf{x}, t) \text{ on } \mathcal{C}. \tag{6.2.10}$$

So we finally have the following equation for the curvature:

$$\sigma \partial_{\hat{\mathbf{s}}} \kappa - \mu_0 \nabla \mathbf{H} \cdot \mathbf{M} \cdot \hat{\mathbf{s}} + \mu_0 \left\{ 1 + \frac{\eta_1 - \eta_2}{\eta_1} \right\} \nabla \times (\mathbf{M} \times \mathbf{H}) \cdot \hat{\mathbf{s}} = 0 \qquad (6.2.11)$$

6.3 Future work

Having established an equation for the curvature, we seek to solve it numerically. There are two major problems to this:

- We do not have an accurate numerical analysis of the magnetization yet.

- We are also somewhat uncertain as to the best scheme for solving (**??**) effectively.

To elaborate, our somewhat crude numerical analysis cannot take into account the magnetic torque term. As this is the term that we wish to consider, solving (**??**) does not accomplish what we would like. However, we hope that in future work one can take into consideration the possible recommendations for numerical analysis of the magnetization, and obtain a better framework in which to solve for the curvature.

However, even with good magnetization data, solving for the curvature is not an easy task. Since the domain we are solving over (in a numerical scheme) necessarily varies with each step, methods are notoriously prone to numerical instability and inaccuracy in the study of thin-film growth in computational soft condensed matter physics. Furthermore, note that the directional derivative itself changes with each step, causing a severe source of computational difficulty. We note that the power of the approach in [15] is that the authors considered a simple expression for magnetization that was reasonable, if not entirely physically rigorous, but allowed them to compute exact solutions so as to avoid this numerical instability.

Finally, we briefly address the issue of extending beyond the no-slip case. In the irrotational case, [26] considered an integral equation for the vortex sheet strength which arises from 6.1.1. Unfortunately we cannot easily extend this sort of analysis as we do not know of a corresponding closed-form expression for the velocity outside of the vortex sheet when the flow is no longer irrotational. Without this, the problem becomes considerably more difficult.

Chapter 7

The pressure Poisson moving boundary value problem

Recall in Chapter 3 we showed that the pressure of our system is given by the solution of a moving boundary value problem. We recall the pressure Poisson equation:

$$\nabla^2 p = \mu_0 \nabla \cdot (\nabla \mathbf{H} \cdot \mathbf{M}) \text{ in } \mathcal{D}, \tag{7.0.1}$$

subject to the following boundary conditions on $\partial \mathcal{D}$:

$$p = -\sigma \kappa + p_0 + \int_{\mathbf{0}}^{\mathbf{H}} \mathbf{B} \cdot d\mathbf{H}' \tag{7.0.2}$$

$$\hat{\mathbf{n}} \cdot \nabla p = \frac{\eta_1}{\eta_2} \hat{\mathbf{n}} \cdot (\nabla p_0 + \mu_0 \nabla \mathbf{H} \cdot \mathbf{M}). \tag{7.0.3}$$

Of course, the boundary itself is moving, according to

$$\frac{d\partial \mathcal{D}}{dt} = \hat{\mathbf{n}} \cdot \mathbf{v}\hat{\mathbf{n}}. \tag{7.0.4}$$

We use this information to formulate a more mathematically rigid statement of our problem, closely following but first we introduce relevant definitions and assumptions. We roughly follow Escher and Simonett [5] in our choice of notation and the idea for the formulation of our problem.

7.1 Background

Let $\mathcal{D}$ be an open simply-connected subset of $\mathbb{R}^2$, $\partial\mathcal{D}$ be analytic, with $\partial\mathcal{D}$ moving in a manner to be prescribed later. Let ν be the normal vector field of $\partial\mathcal{D}$. Fix some $a > 0$, then define $\mathfrak{U}^a := \left\{ \rho \in C^2(\partial\mathcal{D}); ||\rho||_{C^2(\partial\mathcal{D})} < a \right\}$. For any $\rho \in \mathfrak{U}^a$ we define the map $\theta_\rho : \partial\mathcal{D} \to \mathbb{R}^2$ by

$$\theta_\rho := \mathrm{id}_\Gamma + \rho\nu \tag{7.1.1}$$

θ_ρ is a C^2-diffeomorphism mapping $\partial\mathcal{D}$ into its image for sufficiently small a. We define $\partial\mathcal{D}_\rho := \mathrm{im}(\theta_\rho)$. Let $\mathcal{D}_\rho$ be the subset of $\mathbb{R}^2$ C^2-diffeomorphic to $\mathcal{D}$ with boundary $\partial\mathcal{D}_\rho$.

To describe the moving boundary in our problem, we wish to find a family of diffeomorphisms from $\mathfrak{U}$. We describe the time-development of the curve Γ_ρ by defining a map $\varrho : [0,T] \to \mathfrak{U}$ which selects a diffeomorphism for each $t \in [0,T]$; we shall denote this diffeomorphism $\rho(t)$. Then $\mathcal{D}_{\rho(t)}$ and $\partial\mathcal{D}_{\rho(t)}$ evolve in time in a C^2 sense. We define the domain of our problem to be the parabolic cylinder

$$\mathcal{D}_{\varrho,[0,T]} := \bigcup_{t\in[0,T]} \left(\mathcal{D}_{\rho(t)} \times \{t\} \right) \tag{7.1.2}$$

with the boundary naturally given by

$$\partial\mathcal{D}_{\varrho,[0,T]} := \bigcup_{t\in[0,T]} \left(\partial\mathcal{D}_{\rho(t)} \times \{t\} \right) \tag{7.1.3}$$

We suppose $\mathcal{D}$ is the unit circle.

Now we define S_ϱ, the defining function for $\partial\mathcal{D}_\varrho$. Choose $a_0 \in (\mathrm{dist}((0,0), \partial\mathcal{D})$ and let

$$\mathcal{N} : \partial\mathcal{D} \times (-a_0, a_0) \to \mathbb{R}^2, \ \mathcal{N}(x, \lambda) := x + \lambda\nu(x).$$

$\mathcal{N}$ is then a smooth diffeomorphism onto its image by an appropriate choice of a_0, we define $\mathcal{R} := \mathrm{im}(\mathcal{N})$. $\mathcal{R}$ is then the neighborhood of points with distance less than a_0 from Γ. We decompose the inverse of $\mathcal{N}$ into $\mathcal{N}^{-1} = (X, \Lambda)$, with $X \in C^\infty(\mathcal{R}, \Gamma)$ and $\Lambda \in C^\infty(\mathcal{R}, (-a_0, a_0))$. $X(y)$ is the nearest point on Γ to y, while Λ is the distance between y and $X(y)$. So, for any $\rho \in \mathfrak{U}$ we define $S_\rho : \mathcal{R} \to \mathbb{R}$ by $S_\rho(y) := \Lambda(y) - \rho(X(y))$. Then $\partial\mathcal{D}_\rho = S_\rho^{-1}(0)$, and S_ρ has the interpretation of being a level curve of some surface with base

$\partial \mathcal{D}_\rho$.

Let us remark on the usefulness of S_ρ. Suppose for now that θ_ρ is smooth on $\partial \mathcal{D} \times (0, T)$, write $\theta(x, t) = \theta_{\rho(t)}(x)$, and let V denote the normal velocity in the direction of ν, the outer unit normal vector field of $\partial \mathcal{D}_{\rho(t)}$. Then

$$V(\theta(x, t), t) := -\frac{\partial_t S_\rho(\theta(x, t), t)}{|\nabla S_\rho(\theta(x, t), t)|}$$

because the normal vector field on $\partial \mathcal{D}_t$ is given by $\dfrac{1}{|\nabla S_p|}\nabla S_p$. So, if we introduce a boundary condition

$$\partial_t S_\rho - \langle \nabla p + a, \nabla S_\rho \rangle = 0,$$

this implies

$$V = -\langle \nabla p + a, \nu \rangle,$$

which is the natural boundary condition we desire. So, with an initial value $\rho_0 \in \mathfrak{U}$, we define our moving value problem of determining a pair p, ρ satisfying

$$
\begin{aligned}
\nabla^2 p &= 0 & &\text{in } \mathcal{D}_{\rho, [0,T]} \\
p &= \sigma \kappa_\rho & &\text{on } \partial \mathcal{D}_{\rho, [0,T]} \\
\partial_n p &= h & &\text{on } \partial \mathcal{D}_{\rho, [0,T]} & & (7.1.4) \\
\partial_t S_\rho - \langle \nabla p + a, \nabla S_\rho \rangle & & &\text{on } \partial \mathcal{D}_{\rho, [0,T]} \\
\rho(0) &= \rho_0 & &\text{on } \partial \mathcal{D}
\end{aligned}
$$

Here, a corresponds to the $\nabla \times (\mathbf{M} \times \mathbf{H})$ torque term in our model, but the real point is that it cannot be expressed as the gradient of a scalar, and is hence cannot be expressed by redefining p. We take a to be a solenoidal vector field. This difference is the primary change from the model discussed in Escher and Simonett's paper.

Proposition 7.1.1. *Let* $\mathrm{Vol}(t)$ *be the volume of* $\mathcal{D}_{\rho(t)}$, *and suppose that* p, ρ *is a smooth solution to* (7.1.4). *Then* $\dfrac{d}{dt}\mathrm{Vol}(t) = 0$.

Proof. We first note that a is solenoidal, so

$$\int_{\partial \mathcal{D}_{\rho(t)}} \langle a, \nu \rangle d\sigma_t = 0$$

61

By direct computation and the divergence theorem,

$$\frac{d}{dt}\mathrm{Vol}(t) = \int_{\partial \mathcal{D}_{\rho(t)}} V d\sigma_t = -\int_{\partial \mathcal{D}_{\rho(t)}} -\langle \nabla p + a, \nu \rangle = -\int_{\partial \mathcal{D}_{\rho(t)}} -\langle \nabla p, \nu \rangle = \int_{\mathcal{D}_{\rho(t)}} \nabla^2 p \, dx = 0$$

$\square$

We remark that the typical area-shrinking property of normal Hele-Shaw flow does not necessarily seem to hold. Computing the time derivative of the area gives

$$\sigma \frac{d}{dt}\mathrm{Area}(t) = \int_{\partial \mathcal{D}_{\rho(t)}} \sigma \kappa V d\sigma_t = -\int_{\partial \mathcal{D}_{\rho(t)}} (p(a + \nabla u)) \cdot \nu d\sigma_t = -\int_{\mathcal{D}_{\rho(t)}} |\nabla p|^2 d\sigma_t - \int_{\partial \mathcal{D}_{\rho(t)}} pa \cdot \nu d\sigma_t$$

Applying the divergence theorem to the last term of this equation gives

$$\int_{\partial \mathcal{D}_{\rho(t)}} pa \cdot \nu d\sigma_t = \int_{\mathcal{D}_{\rho(t)}} \nabla \cdot (pa) d\sigma_t = \int_{\mathcal{D}_{\rho(t)}} \nabla p \cdot a d\sigma_t$$

It is not likely that this expression will be only positive or negative for all time, so we cannot say that $\mathcal{D}_{\rho(t)}$ is area-shrinking or increasing.

7.2 Some interesting open questions

We believe that, although our model is poorly-studied as of now, future work could be both relatively tractable and of legitimate physical and mathematical interest. Here we pose and discuss a few questions whose answers may help with understanding this sort of solenoidal-driven Laplacian pattern formation.

7.2.1 Do there exist finite-time smooth solutions?

At this time we are unable to establish the existence of solutions to the moving boundary value problem. Much of the analytics is complicated by the presence of the inhomogeneity in the velocity term, which prevents many useful bounds from being made either on $S\rho$ or the gradient of p. It may be useful to assume that a is Hölder-continuous[1], particularly since

---

[1] A function $f : D \to \mathbb{X}$, $D, \mathbb{X}$ metric spaces is Hölder continuous if there exists $C, s > 0$ such that for all $x, y \in D$, $d(f(x), f(y))_{\mathbb{X}} < C d(x,y)_D^s$. This is a generalization of Lipschitz continuity.

Escher and Simonett work in the closure of the Banach spaces of bounded uniformly Hölder continuous functions, but as of now we do not know of an extension of their work.

7.2.2   What sort of regularizing affect does a have on solutions to the MBVP?

It is known that (positive) surface tensions terms are regularizing in irrotational Hele-Shaw flow [10]; that is, the moving boundary value problem is well-posed with classical solutions in finite time, and the moving boundary remains analytic in that finite time. If the surface tension is not positive, the problem is *linearly ill-posed*. A problem $Au = f$, where A is a mapping from a topological space U into a topological space F, with $u \in U$ and $f \in F$ is said to be *well-posed* in the sense of Hadamard if it satisfies the following:

- A is a bijection from U to F.

- A^{-1} is continuous.

It is *ill-posed* if it does not satisfy one of those. The moving boundary value problem is *linearly ill-posed* if it is ill-posed on some fixed domain. The regularizing effect of the positive surface-tension term in Hele-Shaw flow gives the guarantee of finite-time existence of solutions. If we do not have surface tension, the type of boundary data is important. We did not consider an injection or suction in the interior of our domain, but in classical Hele-Shaw flow a fluid is either injected or withdrawn from the domain, which is what causes the Saffman-Taylor instability. In the injection case with no surface tension, solutions are well-posed; otherwise they are not [11].

From this observation, it is natural to ask if the solenoidal term a has the same sort of effect. As we have already observed, the extra term changes the qualitative behavior of solutions fairly substantially by removing the area-shrinking property. Of course, surface tension-free Hele-Shaw flow is also known to be area-shrinking, but the existence of dramatic qualitative behaviorial change due to the presence of surface tension terms seems to suggest that there may be many interesting aspects to this inhomogeneity.

In particular, we consider the possibility that the "curling" motion may reduce or outrightly remove the temporal interval of existence asserted to exist by Escher and Simonett, since the map S_rho may fail to be well-defined after some finite time even if the boundary

is C^∞-diffeomorphic to a unit circle. Again, we are completely certain as to the truth of any of this, but we wish to highlight the scores of interesting questions that the a term poses.

As a related aside, we make note an interesting result obtained by Daskalopoulos Lee in [3]: in Hele-Shaw flow, log-concavity of the initial data implies existence of smooth solutions for all time. The authors considered a *free-boundary problem* rather than a moving boundary, which essentially means that they applied overconstrained boundary conditions that can only be satisfied if the boundary is not fixed for all time. This type of analysis suggests that log-concavity of a may be a reasonable starting point.

7.2.3 Can any useful observations be made from considering weak solutions?

Gustafsson [7] seems to have been the first to introduce weak solutions for Hele-Shaw flow. The principal advantage of his weak solution approach is that one does not need *a priori* to assume any particularly strong regularity conditions on the boundary, which even extends to disconnected domains. Furthermore, the approach hinges on analysis of elliptic variational inequalities, which are easier to treat both analytically and numerically. We outline his definition of weak solutions:

- Given a finite positive measure μ on $\mathbb{R}^2$ with compact support, and ω, Ω open subsets of $\mathbb{R}^2$ such that supp$\mu \subset \omega \subset\subset \Omega$, with $\partial\Omega$ smooth, and define $\mathcal{R}_{\omega,\Omega}$ to be the set of all sets D such that ω is compactly contained in D and D is compactly contained in Ω.

- A weak solution is a map $\phi : [0, T] \to \mathcal{R}_{\omega,\Omega}$ mapping t to some subset D_t such that for each t in $[0, T]$ the function $u_t \in H_0^1(\Omega)$ satisfies $\chi_{D_t} - \chi_{D_0} = \nabla^2 u_t + t \cdot \mu$, provided $u_t \geq 0$ and $\langle u_t, (1 - \chi_{D_t}) \rangle = 0$, where χ_S is the indicator function of a set S and the inner product is the standard L^2 inner product.[2]

We can formulate our problem in a very similar way by simply adding an a to the L^2 inner product condition, but we are uncertain if this is useful.

In Gustafsson's approach, he reduces the problem to that of an "obstacle" variational inequality; unfortunately, the analysis of these inequalities strongly relies on the homogeneity

---

[2]There's actually a somewhat technical detail here; $1 - \chi_{D_t}$ is regarded as being in the dual space of $H_0^1(\Omega)$, denoted $H^{-1}(\Omega)$, but the L^2 inner product is essentially the same.

of the inner product condition defined earlier. As of right now, there seems to be no obvious was to extend his results to the inhomogeneous case. This is entirely reminiscent of the same problem we had earlier. Of course, another (more pragmatic) hinderance in this regard is that we were not sufficiently familiar with variational inequalities to further develop this sort of analysis.

However, the primary reason that we did not fully consider this approach is that it did not seem to yield itself quite as easily to a straightforward physical interpretation of the results. While the existence of weak solutions would be a very worthwhile fact to establish, it does not help us as much with understanding how the velocity inhomogeneity a affects the development of the boundary. Some usefulness could be made out of variational inequalities related to the energy of the system, but time constraints prevented this sort of analysis.

7.2.4   Is numerical analysis possible? If so, is it feasible?

In general, the numerical study of moving boundary value problems is quite hard [2]. In some numerical scheme, one has to keep track simultaneously an iteratively moving boundary and evaluated function, which is prone to numerical instability, inefficiency, and inaccuracy. Even elliptic equations, which may be well-posed and converge rapidly on fixed domains, can be quite hard to solve on a moving boundary.

Furthermore, the addition of our solenoidal term prevents the use of a powerful technique in irrotational two-dimension flow, the conformal map. Cebers, Jackson, and Goldstein [19] use a numerical procedure consisting of iterative conformal maps from a unit disk to numerically model the dynamics of pattern formation, so that the program computes an iterated composition of conformal maps. Because their velocity potential was harmonic, this technique is not only well-defined, it also provides nice, easily visualizable result. The method is not particularly efficient, as at the end it must evaluate a long sequence of function compositions. However, it is stable and effective.

Fortunately, a different method has shown admirable success in moving boundary value problems for elliptic and parabolic systems. In [1], Caginalp describes a *phase field* approach to Hele-Shaw flow, along with the related Stefan problem (which can describe, for instance, the melting of ice into water phrased as a moving boundary value problem). Phase-field methods have been quite successful in analyzing moving boundary value problems whose

65

dynamics depends on some sort of sharp difference between two domains. This is an option which we strongly considered, but time constraints prevented us from fully exploring the method.

Chapter 8

Conclusion

Overall, we did not establish the sort of concrete results that we set out to. Our primary impediment was the large amount of time spent analyzing the literature. The most comprehensive book on ferrohydrodynamics is Rosensweig's text [22], but it is already dated and contemporary notation has made his text difficult to parse, as one needs to constantly reconcile Rosensweig's choice with that currently in favor in the literature.

However, we were able to obtain a number of nice results. Broadly, we feel that we have established a powerful framework in which to study the effects of the newly considered torque term on the dynamics of ferrofluids. In developing our model throughout Chapter 3, we feel that very few meaningful concessions had to be made in order to achieve a workable system of equations. Probably the most glaring concession is that of employing Darcy's law, but a wide variety of experiments have supported this assumption on the velocity, such as [21].

In working with the magnetization separately in Chapters 4 and 5, we were able to demonstrate the shortcomings of some common models for tackling the more general case we deal with, and have set up a numerical framework which can be used with more sophisticated models for the magnetic field internal to the ferrofluid.

Likewise, our result on vortex sheets in Chapter 6 leads to what is potentially a quite powerful way of studying the effect of magnetic torque on the geometry of the boundary. It is also a nice hydrodynamic result; simple solutions in rotational flow, even in the two-dimensional case, are rare, and our simple proof of Eq. (6.2.10) uses and develops many tools on vortex sheets which can find use in further analysis.

Finally, although our treatment of the moving boundary value problem in Chapter 7 was limited and rather rudimentary, it is a nice starting point. The formulation we used is analytically sound, and our brief investigation of weak solutions and numerical methods have strong promise for future research.

8.1   Future Plans

One of the first areas that needs future work is in the numerical magnetization results. As previously discussed, the two models we examined lack very important features for a realistic description of the internal magnetic field. If better expressions can be found for the demagnetization, such as those of [18] and [20], the programs in place can be used to very quickly process these models into magnetization results. Once physically reliable magnetization has been achieved, a number of our other derived equations become fully specified.

In particular, once we have a good expression for the time development of the magnetization, we can solve the differential equation for the curvature, (6.2.11), and obtain a reasonable description for the time development of the shape of the boundary. Also, with these expressions, we can formulate a phase field model for the pressure Poisson equation, and solve that as well.

Finally, the weak solutions introduced in [7] seem to be a potential source of tractable analytical results, since we do not need to worry *a priori* about regularity conditions on the boundary. We expect that, possibly given certain bounds on the solenoidal velocity, weak solutions can be obtained, or the formulation can be modified so that they are obtained.

Bibliography

[1] G. Caginalp. Stefan and Hele-Shaw type models as asymptotic limits of the phase-field equations. *Phys. Rev. A.*

[2] J. Crank. *Free and Moving Boundary Problems.* Clarendon Press, Oxford, 1984.

[3] P. Daskalopoulos and K.-A. Lee. All time smooth solutions of the one-phase stefan problem and the Hele-Shaw flow. *Comm. in Part. Diff. Eqs.*, 29(1 & 2):71 – 89, January 2005.

[4] A. J. Dickstein, S. Erramilli, R. E. Goldstein, D. P. Jackson, and S. A. Langer. Labyrinthine pattern formation in magnetic fluids. *Science*, 261(20):1012–1015, August 1993.

[5] J. Escher and G. Simonett. Classical solutions for Hele-Shaw models with surface tension. *Preprint*, 1997.

[6] C. Flament, G. Pacitto, J.-C. Bacri, I. Drikis, and A. Cebers. Viscous fingering in a magnetic fluid. I. Radial Hele-Shaw flow. *Phys. Fluids*, 10(10):2454–2472, October 1998.

[7] B. Gustafsson. Applications of variational inequalities to a moving boundary problem for Hele Shaw flows. *SIAM J. Math. Anal.*, 16(2):279–300, March 1985.

[8] X. He. *Ferrohydrodynamic Flows in Uniform and Non-uniform Rotating Magnetic Fields.* PhD thesis, Massachusetts Institute of Technology, September 2006.

[9] N. J. Hillier and D. P. Jackson. Width of a ferrofluid finger: Hysteresis and a double energy minimum. *Phys. Rev. E*, 75(3), 2007.

[10] T. Y. Hou, J. S. Lowengrub, and M. J. Shelley. Removing the stiffness from interfacial flows with surface tension. *J. Comp. Phys.*, 114:312–338, 1994.

[11] N. Igbida. Hele-Shaw type problems with dynamical boundary conditions. *J. Math. Anal. Appl.*, 335:1061–1078, 2007.

[12] D. P. Jackson and R. E. Goldstein. Hydrodynamics of fingering instabilities in dipolar fluids. *Phys. Rev. E*, 50(1):298–307, July 1994.

[13] S. A. Langer, R. E. Goldstein, and D. P. Jackson. Dynamics of labyrinthine pattern formation in magnetic fluids. *Phys. Rev. A*, 46(8):4894–4904, October 1992.

[14] S. Odenbach, Ed. *Ferrofluids: Magnetically Controllable Fluids and Their Applications*. Lecture Notes in Physics. Springer, 1 edition, January 2003.

[15] R. M. Oliveira, J. A. Miranda, and E. S. G. Leandro. Ferrofluid patterns in a radial magnetic field: Linear stability, nonlinear dynamics, and exact solutions. *Phys. Rev. E*, 77(1), 2008.

[16] F. Otto. Dynamics of labyrinthine pattern formation in magnetic fluids: A mean-field theory. *Arch. Rational Mech. Anal.*, 141:63 – 103, 1998.

[17] S. E. Rhodes, J. A. Perez, S. M. Elborai, S.-H. Lee, and M. Zahn. Ferrohydrodynamic Hele-Shaw cell flows and instabilities with simultaneous DC axial and in-plane rotating magnetic fields. Research summary from http://fluid.ippt.gov.pl/ictam04/text/sessions/docs/FM4/12662/FM4_12662_new.pdf.

[18] J. Richardi, D. Ingert, and M. P. Pileni. Theoretical study of the field-induced pattern formation in magnetic liquids. *Phys. Rev. E*, 66(4), 2002.

[19] J. Richardi and M. P. Pileni. Nonlinear theory of pattern formation in ferrofluid films at high field strengths. *Phys. Rev. E*, 69(1), 2004.

[20] J. Richardi and M. P. Pileni. Towards efficient methods for the study of pattern formation in ferrofluid films. *Eur. Phys. J. E*, 13:99–105, 2004.

[21] C. Rinaldi, A. Chaves, S. Elborai, X. T. He, and M. Zahn. Magnetic fluid rheology and flows. *Curr. Op. Col. Int. Sci.*, 10:141–157, 2005.

[22] R. E. Rosensweig. *Ferrohydrodynamics*. Cambridge Monographs on Mechanics and Applied Mathematics. Cambridge University Press, New York, 1 edition, 1985.

70

[23] R. E. Rosensweig and J. L. Neuringer. Ferrohydrodynamics. *Phys. Fluids*, 7, December 1964.

[24] P. G. Saffman and G. R. Baker. Vortex interactions. *Ann. Rev. Fluid Mech.*, 11:95–112, 1979.

[25] P. G. Saffman and S. G. Taylor, F.R.S. The penetration of a fluid into a porous medium or Hele-Shaw cell containing a more viscous liquid. *Proc. Royal Soc. London A*, pages 312–329, April 1958.

[26] G. Tryggvason and H. Aref. Numerical experiments on Hele-Shaw flow with a sharp interface. *J. Fluid Mech.*, 136:1–30, 1983.

Appendix A

Magnetization Code

A.1 Simulation in FORTRAN77

This is the FORTRAN77 code which calculates the actual values of the x,y and z components of the magnetization in space and time, outputting them in a large string to the named output file. The format of the output file is as follows:

- Integer representing the number of grid spaces per axis per timestep (excluding the origin), N

- Integer representing one more than the number of sampled times (to keep track of the initial condition), k

  {

- Decimal stating the actual value of the time in seconds for the following timestep's data

- k lines of decimals, each the value of the x-component of the magnetization at a spatial location one grid farther out than the previous, starting at $r = 0$

- Same for the y-component

- Same for the z-component

  }

- Several lines of the values of the parameters used in the calculation

Where the braces indicate the set of data within the output file repeated a total of k times. In addition, this copy of the program uses the following parameter values:

- Number of grid spaces (excluding the origin), $N = 512$

- Number of timesamples (excluding the initial condition), numsample = 2000 (note that this is $k - 1$ from the previous listing)

- Total time of simulation, $t = 0.5$

- Timestep of simulation, dt = 10^{-7}

Having said this, the actual program for the first model follows.

`magnetization2.f:`

```
c234567 10        20        30        40        50        60        70e
      program magnet
      implicit double precision(a-h,l,o-z)
      parameter(N=512,dt=0.0000001,t=.5,numsample=2000,tau=.0000041,
     +    xi=0.00242,omega=25,pi=3.1415926535897932)
c
C     THE PARAMETERS SHOULD BE IN MKS, WE WILL ASSUME A CELL CIZE OF
C     5cm DIVIDED INTO N+1 CELLS ALONG THE R AXIS.  DUE TO THE RADIAL
C     SYMMETRY INHERENT IN THE EQUATION, ONLY THIS SINGLE RAY NEED
C     BE CONSIDERED.
c
      dimension xmag(0:N),ymag(0:N),zmag(0:N),
     +    xchange(0:N),ychange(0:N),zchange(0:N),
     +    xmo(0:N),ymo(0:N),zmo(0:N),
     +    a(0:N),langa(0:N)
      integer i,istep,timesteps,stepgap
      double precision mu,Ms
      double precision hone,hthree
c
C     This program calculates the magnetization in our ferrofluid.
c
C     THESE LINES PREPARE SOME MISCELLANEOUS CONSTANTS AND THE OUTPUT
C     FILE.
c
      timesteps = IDNINT(t/dt)
      stepgap = timesteps/numsample
```

```fortran
      write(6,*)stepgap
      open(7,file='magnet2_dt0000001_thalf')
      write(7,*)N
      write(7,*)numsample+1
      mu=pi*4.0D-7
      cone=dt/tau
      ctwo=dt*mu/(4.0D0*xi)
      Ms=0.0244D0/mu
      hone=0.005D0/mu
      hthree=0.025D0/mu
      do i=0,N
         a(i) = mu*57.849D0*((hone*(i*(.05)/N))**2+hthree**2)**(.5)
         langa(i) = (1.0D0/dtanh(a(i)))-(1.0D0/a(i))
      enddo
c
C     THIS SETS UP THE INITIAL CONDITION (No initial magnetization,
C     magnetic field begins along x-axis)
c
      do i=0,N
         xmo(i) = Ms/((hone**2*(i*(.05)/N)**2+hthree**2)**(0.5))*hone*
     *        (i*(.05)/(N+1))*cos(omega*0*dt)*langa(i)
         ymo(i) = Ms/((hone**2*(i*(.05)/N)**2+hthree**2)**(0.5))*hone*
     *        (i*(.05)/(N+1))*sin(omega*0*dt)*langa(i)
         zmo(i) = Ms/((hone**2*(i*(.05)/N)**2+hthree**2)**(0.5))*
     *        hthree*langa(i)
         xmag(i) = 0
         ymag(i) = 0
         zmag(i) = 0
      enddo
c
C     WE WRITE THE INITIAL CONDITION
c
      write(7,*)0.
      do i=0,N
         write(7,*)xmag(i)
      enddo
      do i=0,N
         write(7,*)ymag(i)
      enddo
      do i=0,N
         write(7,*)zmag(i)
      enddo
```

```fortran
c
C      THIS PERFORMS THE NUMERICAL INTEGRATION
c
       do istep = 1,timesteps
          if(mod(istep,stepgap).EQ.0)then
             write(6,*)istep*100./(timesteps)
             write(7,*)istep*dt
             do i=0,N
                write(7,*)xmag(i)
             enddo
             do i=0,N
                write(7,*)ymag(i)
             enddo
             do i=0,N
                write(7,*)zmag(i)
             enddo
          endif
          omt = omega*dt*istep
          do i=0,N
             xmo(i)=Ms/((hone**2*(i*(.05)/N)**2+hthree**2)**(0.5))*hone*
     *          (i*(.05)/(N+1))*cos(omt)*langa(i)
             ymo(i)=Ms/((hone**2*(i*(.05)/N)**2+hthree**2)**(0.5))*hone*
     *          (i*(.05)/(N+1))*sin(omt)*langa(i)
C
             xchange(i)=cone*(xmo(i)-xmag(i))+ctwo*((ymag(i)**2+zmag(i)
     *          **2)*hone*cos(omt)*(i*(.05)/N)-xmag(i)*(ymag(i)*hone*
     *          sin(omt)*(i*(.05)/N)+zmag(i)*hthree))
C
             ychange(i)=cone*(ymo(i)-ymag(i))+ctwo*((xmag(i)**2+zmag(i)
     *          **2)*hone*sin(omt)*(i*(.05)/N)-ymag(i)*(xmag(i)*hone*
     *          cos(omt)*(i*(.05)/N)+zmag(i)*hthree))
C
             zchange(i)=cone*(zmo(i)-zmag(i))+ctwo*((xmag(i)**2+ymag(i)
     *          **2)*hthree-zmag(i)*(xmag(i)*cos(omt)+ymag(i)*
     *          sin(omt))*hone*i*(.05)/N)
          enddo
          do i=0,N
             xmag(i)=xmag(i)+xchange(i)
             ymag(i)=ymag(i)+ychange(i)
             zmag(i)=zmag(i)+zchange(i)
          enddo
       enddo
```

```
c
C      THIS WRITES VALUES USED FOR PARAMETERS FOR FUTURE REFERENCE
c
       write(7,*)'tau = ',tau
       write(7,*)'xi = ',xi
       write(7,*)'omega = ',omega
       write(7,*)'H1 = ',hone
       write(7,*)'H3 = ',hthree
       write(7,*)'Ms = ',Ms
       stop
       end
```

For the second demagnetization model, the program used follows.

```
magnetization3.f:

c234567 10        20        30        40        50        60        70e
       program magnet
       implicit double precision(a-h,l,o-z)
       parameter(N=512,dt=0.0000001,t=.5,numsample=2000,tau=.0000041,
     +     xi=0.00242,omega=25,pi=3.1415926535897932)
c
C      THE PARAMETERS SHOULD BE IN MKS, WE WILL ASSUME A CELL CIZE OF
C      5cm DIVIDED INTO N+1 CELLS ALONG THE R AXIS.  DUE TO THE RADIAL
C      SYMMETRY INHERENT IN THE EQUATION, ONLY THIS SINGLE RAY NEED
C      BE CONSIDERED.
c
       dimension xmag(0:N),ymag(0:N),zmag(0:N),
     +     xchange(0:N),ychange(0:N),zchange(0:N),
     +     xmo(0:N),ymo(0:N),zmo(0:N),
     +     hdx(0:N),hdy(0:N),hdz(0:N),bigd(0:N),
     +     hx(0:N),hy(0:N),hz(0:N),
     +     a(0:N),langa(0:N)
       integer i,istep,timesteps,stepgap
       double precision mu,Ms
       double precision hone,hthree
c
C      This program calculates the magnetization in our ferrofluid.
c
C      THESE LINES PREPARE SOME MISCELLANEOUS CONSTANTS AND THE OUTPUT
C      FILE.
c
```

```
      timesteps = IDNINT(t/dt)
      stepgap = timesteps/numsample
      write(6,*)stepgap
      open(7,file='magnet3_dt0000001_thalf')
      write(7,*)N
      write(7,*)numsample+1
      mu=pi*4.0D-7
      cone=dt/tau
      ctwo=dt*mu/(4.0D0*xi)
      Ms=0.0244D0/mu
      hone=0.005D0/mu
      hthree=0.025D0/mu
      do i=0,N
         a(i) = mu*57.849D0*((hone*(i*(.05)/N))**2+hthree**2)**(.5)
         langa(i) = (1.0D0/dtanh(a(i)))-(1.0D0/a(i))
      enddo
c
C     THIS SETS UP THE INITIAL CONDITION (No initial magnetization,
C     magnetic field begins along x-axis)
c
      do i=0,N
         zmo(i) = Ms/((hone**2*(i*(.05)/N)**2+hthree**2)**(0.5))*
     *        hthree*langa(i)
         bigd(i) = ((2D0*i*(.05)/(.001*N))**2+1D0)**(-.5)-1D0
C     A CELL THICKNESS OF 1mm IS ASSUMED
         xmag(i) = 0
         ymag(i) = 0
         zmag(i) = 0
      enddo
c
C     WE WRITE THE INITIAL CONDITION
c
      write(7,*)0.
      do i=0,N
         write(7,*)xmag(i)
      enddo
      do i=0,N
         write(7,*)ymag(i)
      enddo
      do i=0,N
         write(7,*)zmag(i)
      enddo
```

```
c
C      THIS PERFORMS THE NUMERICAL INTEGRATION
c
       do istep = 1,timesteps
          if(mod(istep,stepgap).EQ.0)then
             write(6,*)istep*100./(timesteps)
             write(7,*)istep*dt
             do i=0,N
                write(7,*)xmag(i)
             enddo
             do i=0,N
                write(7,*)ymag(i)
             enddo
             do i=0,N
                write(7,*)zmag(i)
             enddo
          endif
          omt = omega*dt*istep
          do i=0,N
             xmo(i)=Ms/((hone**2*(i*(.05)/N)**2+hthree**2)**(0.5))*hone*
     *          (i*(.05)/(N+1))*cos(omt)*langa(i)
             ymo(i)=Ms/((hone**2*(i*(.05)/N)**2+hthree**2)**(0.5))*hone*
     *          (i*(.05)/(N+1))*sin(omt)*langa(i)
C
             hdx(i)=bigd(i)*xmo(i)
             hdy(i)=bigd(i)*ymo(i)
             hdz(i)=bigd(i)*zmo(i)
C
             hx(i)=hone*cos(omt)-hdx(i)
             hy(i)=hone*sin(omt)-hdy(i)
             hz(i)=hthree-hdz(i)
C
             xchange(i)=cone*(xmo(i)-xmag(i))+ctwo*((ymag(i)**2+zmag(i)
     *          **2)*hx(i)-xmag(i)*(ymag(i)*hy(i)+zmag(i)*hz(i)))
C
             ychange(i)=cone*(ymo(i)-ymag(i))+ctwo*((xmag(i)**2+zmag(i)
     *          **2)*hy(i)-ymag(i)*(xmag(i)*hx(i)+zmag(i)*hz(i)))
C
             zchange(i)=cone*(zmo(i)-zmag(i))+ctwo*((xmag(i)**2+ymag(i)
     *          **2)*hz(i)-zmag(i)*(xmag(i)*hx(i)+ymag(i)*hy(i)))
          enddo
          do i=0,N
```

```
            xmag(i)=xmag(i)+xchange(i)
            ymag(i)=ymag(i)+ychange(i)
            zmag(i)=zmag(i)+zchange(i)
         enddo
      enddo
c
C     THIS WRITES VALUES USED FOR PARAMETERS FOR FUTURE REFERENCE
c
      write(7,*)'tau = ',tau
      write(7,*)'xi = ',xi
      write(7,*)'omega = ',omega
      write(7,*)'H1 = ',hone
      write(7,*)'H3 = ',hthree
      write(7,*)'Ms = ',Ms
      stop
      end
```

A.2   Data Processing in MATLAB

This is the MATLAB m-file which was written to process the output from the FORTAN
programs. The program automatically generates a number of movies in time which may
then be exported, as well as a number of smaller matrices within MATLAB which may then
be plotted manually as desired. Suggested use is given in the help file for the program. It
is worth noting that MATLAB's storage format for movies causes this program to require
a very large amount of memory, more than 4 GB in our tests, and these lines should be
removed for use on most systems.

```
function [Mx,My,Mz,Mxy,X,Y,Z,R,t,space] = magnet(file)
% This function does the data processing and curve fitting for the
% magnetization analysis for the MQP.  The outputs starting with 'M' are
% the movies produced, while the rest are the actual processed data from
% which manual plots may be produced.  As an example, this program may be
% used on the default output of magnetization2.f by typing
% '[Mx,My,Mz,Mxy,X,Y,Z,R,time,space]=magnet('magnet2_dt0000001_thalf')',
% omitting the outermost quotes, in the command window.

% Note: In order for this command to work with the output from the
% simulation, the Java VM heap space had to be increased to 2048m by
% putting a file called java.opts in $MATLABROOT/bin/$ARCH, the sole
```

```
% contents of which was the line "-Xmx2048m" (without quotes).  $MATLABROOT
% and $ARCH can be discovered through the commands matlabroot and
% computer('arch') in the command window.  Further note that my computer
% had over 4GB of RAM in use after the file was opened.
input = fopen(file);
if input == (-1)
    error('Cannot open file')
end
Nspace = fscanf(input,'%d',1)+1;
Ntime = fscanf(input,'%d',1);
X = zeros(Nspace,Ntime);
Y = zeros(Nspace,Ntime);
Z = zeros(Nspace,Ntime);
t = zeros(Ntime,1);
space = linspace(0,0.05,Nspace)';

% These lines split the data into the actual components of the
% magnetization of the form X(space,time), as well as creating a vector t
% which stores the actual time in seconds of the simulation in the entry
% corresponding to a time index for any of the magnetization matrices.
for j=1:Ntime
    t(j) = fscanf(input,'%g',1);
    for i=1:Nspace
        X(i,j) = fscanf(input,'%g',1);
    end
    for i=1:Nspace
        Y(i,j) = fscanf(input,'%g',1);
    end
    for i=1:Nspace
        Z(i,j) = fscanf(input,'%g',1);
    end
end


R = (X.^2+Y.^2).^(0.5);
% We want to make some movies to visualize the behaviour of the various
% magnetization components in time
for k = 1:Ntime
    plot(space,X(:,k))
    axis([0 0.05 -100 100])  %use -100 to 100 for magnet2, -210 to 210 for magnet3
    Mx(k) = getframe;
end
for k = 1:Ntime
```

```
    plot(space,Y(:,k))
    axis([0 0.05 -100 100])  %same bounds as x
    My(k) = getframe;
end
for k = 1:Ntime
    plot(space,Z(:,k))
    axis([0 0.05 0 8500])
    Mz(k) = getframe;
end
for k = 1:Ntime
    plot(space,X(:,k))
    axis([0 0.05 -100 100])  %same bounds as x
    hold on
    plot(space,Y(:,k),'red')
    plot(space,R(:,k),'green')
    Mxy(k) = getframe;
    hold off
end
```